

**NIST-GCR-96-704**

---

---

**FLAME BASE STRUCTURE OF SMALL-SCALE  
POOL FIRES**

---

---

**S. Venkatesh, A. Ito, K. Saito**

**Department of Mechanical Engineering  
University of Kentucky  
Lexington, KY 40506-0108**

**and**

**I.S. Wichman**

**Department of Mechanical Engineering  
Michigan State University  
East Lansing, MI 48824-1226**

**December 1996**



**U.S. Department of Commerce  
Michael Kantor, *Secretary*  
Technology Administration  
Mary L. Good, *Under Secretary for Technology*  
National Institute of Standards and Technology  
Arati Prabhakar, *Director***

### Notice

This report was prepared for the Building and Fire Research Laboratory of the National Institute of Standards and Technology under grant number 60NANB4D1674. The statement and conclusions contained in this report are those of the authors and do not necessarily reflect the views of the National Institute of Standards and Technology or the Building and Fire Research Laboratory.

This paper was presented at:  
the 26th International Symposium on Combustion, 1996 and  
will appear in the Proceedings.

**Flame Base Structure of Small-Scale Pool Fires**

**S. Venkatesh, A. Ito, K. Saito<sup>\*</sup>**

*Department of Mechanical Engineering  
University of Kentucky  
Lexington, KY 40506-0108*

**and**

**I.S. Wichman**

*Department of Mechanical Engineering  
Michigan State University  
East Lansing, MI 48824-1226*

<sup>\*</sup> Corresponding Author: K. Saito  
Tel (606)257-1685, Fax (606)257-3304

**Current Addresses:**

- (1) A. Ito, Dept. of Production Systems Engineering  
Oita University, Oita, Japan
- (2) S. Venkatesh, Acurex Environmental Corp.,  
555 Clyde Avenue, P.O. Box 7044  
Mountain View, CA 94039

**Colloquium Topic:  
Fundamentals of Fire Research**

# FLAME BASE STRUCTURE OF SMALL SCALE POOL FIRES

S. Venkatesh, A. Ito, K. Saito  
University of Kentucky

and

I.S. Wichman  
Michigan State University

## ABSTRACT

This paper attempts to answer the question, "Why are small scale pool fires anchored?" by providing and interpreting a new set of experimental data. For momentum-controlled, high Reynolds ( $Re$ ) number turbulent-jet diffusion flames, the formation of a premixing zone is suggested as the primary reason for the flame anchoring. For buoyancy-controlled pool fires, however, the existence of the premixing zone at the flame base is not clear because both  $Re$  and  $Fr$  (Froude number) are low. To improve our understanding of the flame anchoring mechanism and structure of buoyancy-controlled liquid pool fires, we employed small scale pool fires whose diameters range between 1.5 – 20 cm. Our measurements include flow visualization by a particle-track laser-sheet technique (PTLS) combined with a high speed video camera and temperature profiles by a fine thermocouple. We found from those measurements that major air entrainment occurred through the primary anchoring zone, PAZ, which consists of a small area covering approximately 1 cm high and around the circumference just above the dark zone; while air entrainment through the quenching zone (a dark zone formed between the visible flame edge and the burner port) was negligible. The structure of the PAZ was found to be premixed flame (another interpretation may be it is similar to counter-diffusion flame). This enables the pool fires to anchor at the burner port. In addition, we visualized the existence of a vortex ring at a stagnation zone in the fuel vapor phase for both propanol and hexane pool fires, in agreement with qualitative observation by other workers.

## INTRODUCTION

The mechanism of air entrainment in pool fires is of current interest because of both fundamental curiosity and practical concerns related to flame extinguishment by liftoff through flame blowoff and flame instability near the burner port. In past research on buoyancy controlled pool fires, McCaffrey [1] and Cox and Chitty [2] proposed three separate zonal structures (Fig. 1): a continuous flame zone as the base of the flame, which is followed by an intermittent flame zone where active turbulent mixing takes place, and above it a plume zone where the center-line temperature begins its decrease.

Weckman and associates [3–5] performed a simultaneous measurement of velocity and temperature profiles in and around medium sized pool fires whose diameters ranged from 30 cm to 60 cm. Zhou and Gore [6] and Cetegen [7] studied flow structures of pool fires induced by buoyancy. Zhou and Gore [6] performed a series of elaborate laser-Doppler-velocimetry (LDV) and particle-image-velocimetry (PIV) measurements and obtained a velocity map around a liquid pool fire of 7.1 cm diameter. Cetegen [7] developed his unique optical measurement system and obtained a series of phase resolved velocity fields for pulsating buoyant plumes of helium-air mixtures over a 10 cm diameter nozzle. Cetegen found that the flow structure of buoyancy controlled pool fires can be simulated by helium flow moving upwardly against a quiescent air environment. The above studies [1–7] help us understand the mechanisms of flame pulsation, air entrainment, and air-fuel mixing in buoyancy controlled pool fires.

Here, we attempt to understand the mechanism of flame anchoring at the base. Our focus, therefore, differs from [1–7] and is more closely related to that of Bouhafid et al [8], who measured temperature, and species ( $\text{CO}$ ,  $\text{CO}_2$  and  $\text{O}_2$ ) concentration profiles for a 15 cm diameter kerosene pool fire. Bouhafid et al. [8] observed a looped isotherm by a fine thermocouple and looped iso- $\text{CO}$  and iso- $\text{CO}_2$  concentrations by a stainless steel, water cooled aerodynamic quench probe followed by an online gas chromatography analysis. They suggested that air entrainment near the base leads to fuel-air mixing by

convection giving the flame a premixed character causing pool fires to be anchored. However, their oxygen concentration profiles near the edge of the flame may not be reliable because their probe quenches chemical reactions around the probe and thereby creates a quenching area through which air can diffuse into the flame interior.

We believe that their premixing mechanism can be accurately examined using a non-intrusive flow visualization technique. Indeed, Bouhafid et al [8] made an attempt to visualize their 15 cm kerosene pool fire, but their effort was unsuccessful because of strong emissions from the kerosene flame. Therefore, we chose hexane and propanol because they are less sooty than kerosene. We conducted flow visualization, P-TLS-velocity and thermocouple-temperature measurements in order to reveal detailed flow and temperature structures at PAZ.

Our objectives are:

(1) Understanding the mechanism of flame anchoring in pool fires. We investigate if and how the PAZ controls the flame anchoring. The cross-sectional area of PAZ is at most 1 cm high x 1 cm wide in radial direction consisting of the pan's brim surface, a sub-millimeter size dark (quenching) zone, a millimeter-size visible leading flame edge, and an extended (believed to be diffusion controlled) flame zone. We divided McCaffray's continuous flame zone into three subzones: the quenching zone, PAZ, and post PAZ, and studied each zone thoroughly. Figure 1 shows a schematic of the five-zone structure.

Much work has been conducted on the stability and liftoff of laminar and turbulent jet diffusion flames. The common understanding is that premixing occurs near the base and is responsible for anchoring and stabilization. The results by Takahashi et al. [9,10] on turbulent jet diffusion flames show mixing of the fuel and air through a circulation zone established at the burner rim due to strong shear stresses, leading to flame anchoring. For liquid pool fires, Bouhafid et al [8] suggested the formation of a premixed reaction zone as the mechanism of flame anchoring due to the observed strong radial component of the air velocity induced by the plume. We think that in a pool fire, the fuel

and oxidizer velocities at PAZ are much smaller, perhaps insufficient to produce shear stress induced circulation zones observed for the turbulent jet diffusion flames.

(2) Understanding of the mechanism of air entrainment at PAZ and other heights. According to Bouhafid et al [8] and this study, convective air entrainment likely occurs at PAZ in order to satisfy mass conservation because of the rapid acceleration of the buoyant gases in the flame interior. In the intermittent region, however, air entrainment occurs mainly by relatively large-scale buoyancy-induced mixing as explained by Weckman et al [3-5], Zhou and Gore [6] and Cetegen [7]. In the post-PAZ region where the flame is a pseudo laminar continuous flame, air streamlines are parallel to the visible flame surface (to be shown in Fig. 3), and air transport to the flame surface is by diffusion.

(3) Experimental confirmation of the stagnation and re-circulation zone. Based on thermocouple temperature and CO, CO<sub>2</sub> concentration measurement data, Bouhafid et al [8] predicted the existence of a stagnation and re-circulation zone in the fuel-vapor phase just above the liquid fuel surface. Yet there is no experimental data to directly verify their prediction; therefore, flow-visualization experiments were conducted in order to examine the proposed stagnation and re-circulation zones.

## **EXPERIMENTAL METHODS**

Pool fire experiments were conducted at the pan's wall temperature at  $20 \pm 2$  °C by wrapping the pan's outer wall with a 4 mm diameter copper tube and circulated water through the tube. We found the pool fire was most stable when the fuel level was 0.5 mm below the brim. Therefore, we first filled the fuel to the brim, ignited it by a small propane torch, allowed the fuel level to decrease by 0.5 mm, and applied a liquid-level controller to keep the fuel level at that position. To investigate the dependence of the flow structure on the pool diameter, stainless-steel pans of six different diameters (1.5, 3.3, 5.7, 7.8, 10 and 20 cm) and 2 cm height were designed. In this diameter range, all

the pool fires exhibited a similar flame structure shown in Fig. 1. Then, detailed measurements were conducted using the 5.7 cm diameter pan.

### **Flow Visualization and Velocity Measurement**

We learned from the exploratory experiments that a particle-track laser-sheet technique with a high speed video camera (500 frame/s and 25 degree view angle) system (PTLS) can serve best for our measurements, because PTLS can measure profiles of both stream lines and the 2D velocity with significantly fewer particles and nearly instantaneously [11]. If the flow field is in a steady state, a 3D flow field can also be measured by rotating the cylindrical lens about the laser beam. We first checked our flow structure using this method and found that our flow profiles at PAZ are co-axial, i.e., the velocity vector possesses only the  $r$  and  $z$  components (a schematic of the experimental apparatus is shown in Fig. 1 and the flow visualization result will be presented later).

Using a 300 mW Argon-ion laser beam and a cylindrical lens, we established a thin laser sheet with an approximately 35 degree opening angle (Fig. 1). Pool fires were seeded with commercially available talc particles (its mean diameter was determined to be  $3 \pm 1 \mu\text{m}$  by SEM). The air stream was seeded by talc particles generated by a seeding bed located 5 cm below and away from the pan's rim (Fig. 1). To visualize the buoyancy-induced flow inside the flame sheet, a 0.5 cm diameter stainless-steel tube was welded in the co-axial location of the 5.7 cm diameter pan through which talc particles were slowly injected into the flame. Both the burning rate of fuel and the visible flame height remained unchanged with and without the seeding tube. Furthermore, we visualized the fuel-vapor flow in the flame interior near the fuel surface by seeding particles through the quenching zone and comparing these results to the above results. We did not find any difference in the results obtained by these two techniques, thus confirming that a particle injection-velocity of 7 cm/s and our low number density particles produced no significant changes in the original flow field.

## Temperature Measurement

Temperature measurements were made using a 75  $\mu\text{m}$ -diameter uncoated chromel–alumel thermocouple. The thermocouple was not coated because there was no difference in the temperature reading with and without the silica coating in PAZ. The effects of the conductive heat loss (or gain) through the wire and the convective heat loss (or gain) from the wire and the couple bead were estimated to cause a temperature difference in the neighborhood of 100 – 150K, and radiation heat loss to be approximately 100 K temperature drop at the flame sheet using [12]. Because temperature fluctuations are negligible at PAZ and our pool fires produce less soot, the effect of soot deposition on the thermocouple was negligible except for a narrow (the center of the downward-pointing horn) region of the hexane flame. The best possible thermocouple shape and its insertion angle for our pool fires were experimentally determined (see Fig. 1 for a schematic).

## RESULTS

### Flame Appearance

A clear blue flame attaches 0.2 mm above the port, it extends 0.8 to 1 cm from the port, and it becomes invisible beyond that height. Then, a yellow luminous flame with a downward-pointing horn shape begins. There is a small range of heights where both the blue flame and the yellow flame existed. Above that zone, a luminous continuous flame followed. The double flame structure, shown in Figs. 3 and 4, was previously observed for ten different hydrocarbon–air diffusion flames under laminar over-ventilated coflow air conditions [13].

We confirmed the formation of a blue whisker flame (possibly part of a triple flame) for hexane and propanol pool fires. Then, our effort was further extended to six different fuels (methanol, acetone, pentane, octane, decane, and benzene). Because of the strong luminosity, the formation of the blue whisker flame was not clear for benzene. So,

a 1.6 cm diameter Pyrex coflow apparatus with an evaporator in the fuel line (detailed in [14]) was used and a benzene-air diffusion flame of 2 cm flame height was established. The fuel was then diluted by nitrogen. With 5 to 6 times nitrogen (by volume) dilution, the flame became less luminous and the formation of the double-flame structure became clearly identifiable.

As a result, the formation of the double-flame structure has been confirmed for 19 different fuels (hydrocarbons and alcohols) for the diameter ranges from 1 to 10 cm with and without nitrogen dilution.

### Flow and Temperature Structures

For the 5.7 cm diameter propanol fire, flow structures of the air entrainment and the fuel-vapor are shown in Fig. 2, and a flow-vector diagram constructed from figures 2 results is shown in Fig. 3. Figure 4 shows a schematic of the double flame structure and tangential  $V_t$  and normal  $V_n$  components of the particle velocity  $V$  along the flame sheet as a function of vertical height from the burner port. The same measurements were conducted for the hexane pool fire, but they were not presented here because they behaved similarly.

Air entrainment through the visible flame sheet occurs just above the pan's brim and continues approximately 0.8 mm to 1 cm above the port (Fig. 3). Air entrainment at PAZ is by a smooth laminar flow suction as opposed to the intermittent zone, where it occurs by large-scale buoyancy-induced mixing. In the post-PAZ, air entrainment is only by diffusion as the velocity vectors indicate in Fig. 3. For both propanol and hexane, the ratio of air entrainment through the quenching zone to the net air entrainment at PAZ was found to be approximately 0.05.

### DISCUSSION

The observed PAZ structure, where a substantial amount of air penetrates the

flame sheet by convection suggesting it can be either interpreted as premixed flame or counter-flow diffusion flame [15,16]. The authors provide experimental data on which these two interpretations based, but do not conclude which interpretation is more feasible and encourage future research on this problem.

The theoretical structure of the flame near the base or the burner rim resembles a wall-quenched triple (or tribrachial) flame, whose character has been discussed [17,18]. The general requirement is for two initially separated streams of fuel and oxidizer, which mix by molecular diffusion after flowing past a divider. Enhanced mixing may be promoted by the partial premixing of one or both reactant streams. In theory, the resultant flame structure consists of an intersection of two variable-strength premixed flames (PFs), one lean, the other rich, with a flame whose locus coincides with the stoichiometric line. The point of intersection is called the triple point (TP). Here the reaction rate is a maximum, with a value far higher than the two PF arcs. The intensely localized region of high reaction rate allows the flame structure to survive, despite the nearby hostile environment of a quenching surface. Interestingly, the gradient of the reaction rate toward the quenching surface is so high that the location of maximum reaction rate practically coincides with the quench point.

The position of the flame locus may shift depending on the overall stoichiometry. In the usual case, the flame lies on the oxidizer side in the mixture fraction coordinate  $Z$ , where  $Z = 0$  in the pure oxidizer stream and  $Z = 1$  in the pure fuel stream (either of which may be fictitious), and  $Z = Z_f = 1/(1 + \nu)$  at the DF locus. When  $\nu$  is either greater or smaller than unity, one of the two PFs may be smaller than the other, depending also on the local flow field. In the flow field examined in Fig. 3, we see that the oxidizer-side flow entering the flame is substantial, whereas the fuel-side flow is negligible. Hence, regardless of the  $\nu$ -value, the fuel-side PF must be small since there is no flow against which it may propagate. The oxidizer-side PF, however, propagates against the vigorous entrained air flow. Therefore, the oxidizer-side PF is by far the

more vigorous. This argument may explain the double-flame structure that is observed, although blockage of the small fuel-side flame may hamper visualization.

Concerning stoichiometry, we observed that the six fuels examined here are methanol ( $\nu = 1.5$ ,  $Z_f = 0.4$ ), propanol ( $\nu = 4.5$ ,  $Z_f = 0.182$ ), acetone ( $\nu = 4.5$ ,  $Z_f = 0.182$ ), pentane ( $\nu = 8$ ,  $Z_f = 0.111$ ), hexane ( $\nu = 9.5$ ,  $Z_f = 0.0952$ ), and octane ( $\nu = 12.5$ ,  $Z_f = 0.0741$ ), all of which have  $\nu > 1$  and  $Z_f < 0.5$ . Color photographs of the flame in the air entrainment zone were taken, their images were projected on a screen, and their relative positions were measured [19]. As  $\nu$  increases and  $Z_f$  decreases, the entrainment-zone diameter  $d$  increased as the flame moved toward the oxidizer side (smaller  $Z_f$ ):  $d_{\text{oct}} > d_{\text{hex}} > d_{\text{prop}} > d_{\text{acet}} > d_{\text{meth}}$ . Hence, the observed flame structure is consistent with the nature of the flow field and the change of flame position is consistent with the stoichiometry. Note that, however, acetone (molecular weight, 58.05) and 1-propanol (molecular weight, 60.09) possess different air-entrainment-zone diameters. This suggests that beside the effect of stoichiometry,  $\nu$ , often parameters like pyrolysis rates, preferential diffusion, flame temperature and burning rates also influence the location of the flame sheet.

### **Why is the Double Flame Instead of the Triple Flame Observed?**

We observed the double flame instead of the triple flame. This fact needs to be discussed here. A rather detailed discussion of triple (or tribrachial) flame propagation into an opposing flow of partially premixed gases has been given by Chung and Lee [20], who argue that the tribrachial flame propagates with a speed very close to the stoichiometric flame speed. This hypothesis has some theoretical support from the calculations of Dold [21] and others for the case of free or isenthalpic flames far from cold surfaces. Near cold surfaces, where the flame may suffer substantial enthalpy losses, this hypothesis breaks down entirely. In fact, flames may attach without any opposed flow at all. That is, pure diffusion flames can attach to cold and chemically frozen regions simply

through the creation of upstream mixing regions (formulas for the quenching distance were given [17]).

Regarding the above question, it is important to pay attention to the fact that the velocity of air flow in the air side is one order of magnitude higher than the velocity of fuel vapor in the fuel side and the visible flame sheet is located in the air stream side. Although a relatively strong air current is crossing the flame sheet and convecting into the flame interior (Figs. 3 and 4), the fuel vapor will eventually diffuse to the flame. Thus, the oxidizer side PF is expected to be much larger than the fuel side PF. As demonstrated in Figs. 2 and 3, the flame at PAZ possesses characteristics of the counter diffusion flame, yet the existence of the cold wall quenches the flame and likely to distort the normal (or free boundary) triple flame into the double flame.

### **Temperature Structure**

Radial temperature profiles at different heights are shown in Figs. 5a and 5b; both fuels exhibit a steep temperature gradient on the air side. The flame sheet temperature (peak temperature) is greater for n-hexane than 1-propanol near the base. The measured temperature near the base appears to be consistent with recent theoretical results [22], which showed an extinction temperature, 1230 °C based on three step chemical reactions rather than a one-step overall reaction. In the yellow (sooty) region,  $z = 5$  and 10 mm in Figs. 5a and 5b, the flame sheet temperature of propanol is greater than hexane. This may be because of the larger radiation losses and uncertainties in the thermocouple temperature measurements in the hexane flame where the thermocouple was coated (only at the limited location,  $Z = 10$  mm in Fig. 5a) with soot particles causing a rapid decrease in its output reading.

### **Flame Anchoring Mechanism**

Takahashi and Schmoll [10] have shown that for the turbulent jet diffusion flames,

the mechanism of anchoring depends on the formation of shear-stress related circulation zones. Due to shearing between the fuel jet, whose flow speed may be much higher than the flame propagation speed, and the oxidizer, a stagnant circulation zone is developed where mixing occurs and the flame is allowed to anchor. They proved that when a burner with a tapered rim was used, the flame was not able to anchor or stabilize. However, our data show that in a pool fire, the shear stresses at the rim are lower by two orders of magnitude compared to the jet diffusion flame [10] demonstrating insignificance of shear-stress induced mixing. This suggests that the mechanism of anchoring of a flame in a buoyancy dominated pool fire and a momentum-force dominated jet diffusion flame are different. Nevertheless, both anchoring mechanisms require the generation and sustained presence of a mixing zone, where fuel and oxidizer can intermix. The mechanisms by which these two flames produce these zones are quite distinct.

We believe that in PAZ the structure of the flame sheet is similar to a triple flame although only the double structure was observed here. Because of finite-rate chemistry influences, the flame sheet has a finite thickness. Because the DF is bounded on either side by two PFs, we may introduce the concept of the flame propagation speed. We focus on the outer (oxygen-rich) PF. The direction of the flame propagation vector is opposite to the tangential component of the entrainment vector,  $V_t$ . If  $V_t$  is greater than the flame propagation speed near the base, the flame won't be able to anchor or stabilize, as shown by Takahashi and Schmoll [10] by using a tapered burner. We confirmed from our PTLs measurements (Figs. 3 and 4) that  $V_t$  in the convective-air entrainment zone was lower than the stoichiometric flame speeds (propanol, 0.34 m/s and hexane 0.42 m/s).

To experimentally prove this, we designed a 15 cm diameter Pyrex-chimney and attached it to the 5.7 cm-diameter pool fire burner in a coaxial location. The aim of this experiment is to prove that when the air velocity exceeds  $V_t$ , the pool fire will lift off from the base. This burner system was designed based on the concept of our coflow hydrocarbon-air diffusion-flame burner [13]. The air was supplied from a compressed air

cylinder through an air filter; its volumetric flow-rate was controlled and measured by a rotameter. Normal propanol and hexane were used as fuel, external air was seeded by the talc particles, and the  $r$ - $z$  velocity components of air at and near PAZ was measured by PTLs. Our experiments demonstrated that the pool fires can anchor at the burner rim provided the tangential component of the air velocity  $V_t$  is less than approximately 0.3 m/s (because of the page limitation, the data is not presented here and see ref. [19]). With the slight increase of  $V_t$ , the flame suddenly become unstable causing a sudden liftoff of the flame, and sometime causing reattachment of the flame to the rim. With further increase of  $V_t$ , a steady lift-off of the flame occurred. The flame can be anchored at the rim or it can be lifted-off to the height where the main flame begins. The leading edge of the flame was quite unstable at PAZ and could not anchor at any PAZ region [19].

## SUMMARY AND CONCLUSIONS

In reference to the three specific objectives addressed in the **Introduction**, the conclusions obtained from this study are summarized here.

(1) Based on our experimental measurements on pool fires in diameter of 1.5 – 20 cm of propanol and hexane, and finite-rate chemistry concepts, the entire flame sheet of a pool fire is established to have a triple flame structure. The structure of the flame at the base was established from PTLs data and through a comparison of the location of the flame sheet in the convective-air entrainment zone for fuels with different stoichiometric fuel-air requirements.

(2a) Air entrainment through the quenching zone was found to be a small fraction of the net air entrainment near the base for the pool fires. Our data show that the ratio of the total mass of air entrained into the flame interior through PAZ to the total mass of air entrained through the quenching zone was 0.05.

(2b) The fluid-dynamic structure of the anchoring mechanism of a

buoyancy-dominated small scale pool fire and a momentum-dominated jet diffusion flame is different. In a jet diffusion flame, the Reynolds shear stress near the rim of the burner induces a stagnant re-circulation zone where the fuel and the oxidizer are mixed and the flame anchors. To the contrary, in a pool fire the shear stresses at the rim are two orders of magnitude lower and turbulent mixing does not occur [23]. Finite-rate chemistry establishes the presence of a molecular-diffusion mixing zone. Therefore, the flame anchors at the base.

(3) For both propanol and hexane pool fires with their diameter range between 1.6 cm and 10 cm, the formation of the stagnation re-circulation zone predicted by Bouhafid et al [8] was experimentally confirmed.

#### **ACKNOWLEDGEMENTS**

We would like to thank F.A. Williams, A.S. Gordon and T. Hirano for their valuable comments. This study was supported in part by the National Institute of Standards and Technology under grant #60NANB4D1674, in part by NASA-Kentucky EPSCoR program and in part by the Center for Manufacturing Systems at the University of Kentucky.

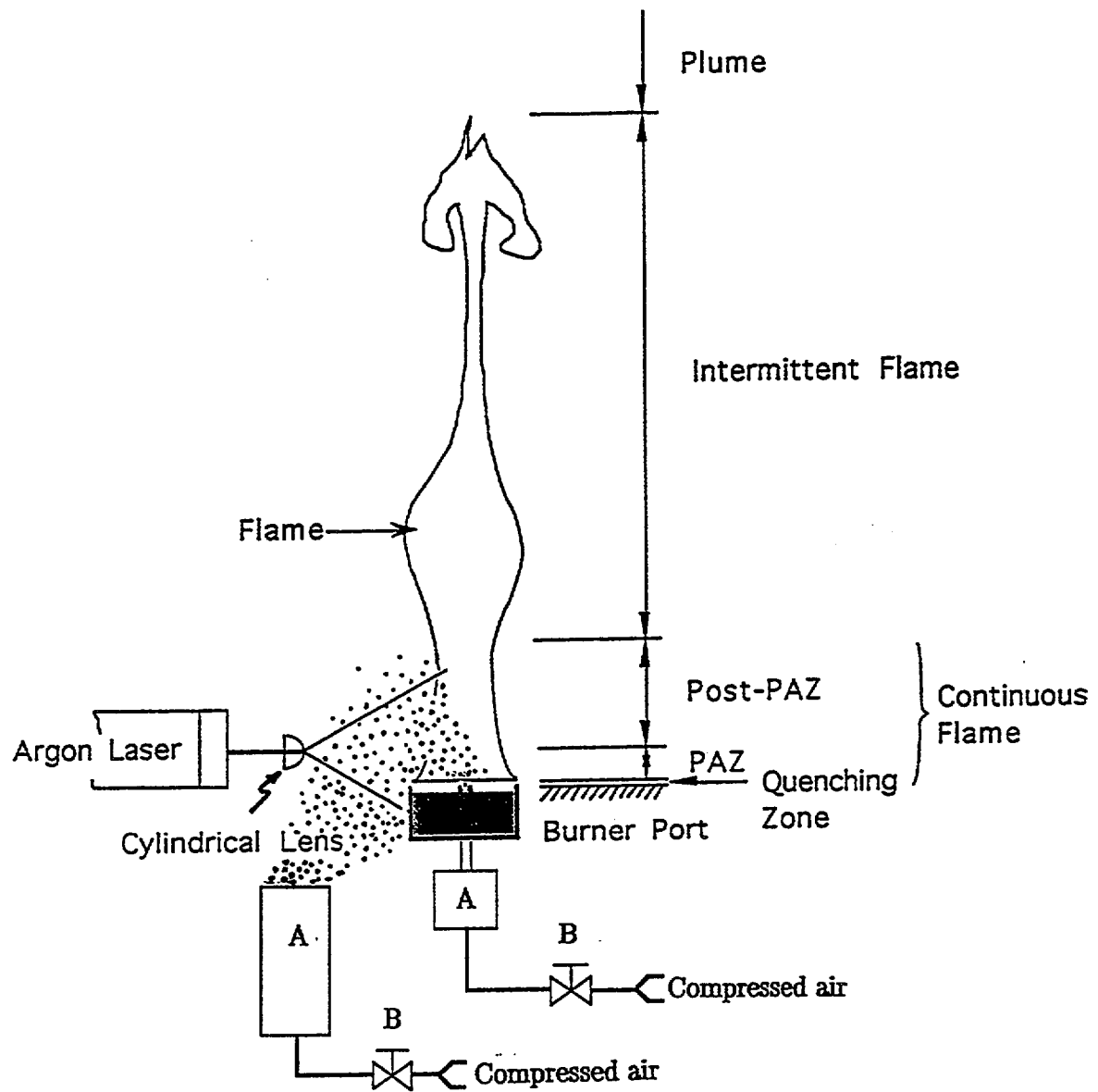
## REFERENCES

1. McCaffrey, B.J., *Combustion and Flame*, 52: 149–167 (1983).
2. Cox, G. and Chitty, R., *Combustion and Flame*, 39: 191–209 (1980).
3. Weckman, E.J., *Ph.D. Thesis*, University of Waterloo, Ontario, Canada, 1987.
4. Weckman, E.J. and Sobiesiak, A, *Twenty-second International Symposium on Combustion*, The Combustion Institute, 1988, pp. 1299–1310.
5. Weckman, E.J. and McEwen, C.S, *ASME/JSME Joint Thermal Engineering Conference*, Vol. 5, 1991.
6. Zhou, X.C., and Gore, J., *Combust. Flame*, 100: 52–60 (1995).
7. Cetegen, B., "Phase-resolved Velocity Field Measurements in Pulsating Buoyant Plumes of Helium–Air Mixtures," presented at the *Annual NIST Fire Research Conference*, Gaithersburg, MD., October 20, 1994.
8. Bouhafid, A., Vantelon, J.P., Joulain, P. and Fernandez-Pello, A.C., *Twenty-second International Symposium on Combustion*, The Combustion Institute, 1988, pp. 1291–1298.
9. Takahashi, F., Mizomoto, M., Ikai, S., and Futaki, N., *Twentieth International Symposium on Combustion*, The Combustion Institute, 1985, pp. 295–302.
10. Takahashi, F. and Schmoll, W.G., *Twenty-third International Symposium on Combustion*, The Combustion Institute, 1990, pp. 677–683.
11. Hirano, T., Sato, K. and Tazawa, K., *Combust. Flame*, 26: 191–200 (1976).
12. Kaskan, W.E., *Tenth International Symposium on Combustion*, The Combustion Institute, 1960, pp. 134–143.
13. Saito, K., Williams, F.A., and Gordon, A.S., *Combust. Sci. Tech.*, 51: 291–312 (1987).
14. Sidebotham, G., Saito, K. and Glassman, I., *Combust. Sci. Tech.*, 85: 283–296 (1991).
15. Williams, F.A. *Combustion Theory*, Benjamin/Cummings, 1985.
16. Tsuji, H., *Prog. Energy and Combust. Sci.*, 8: 93–119 (1982).
17. Wichman, I.S., *Combust. Sci. Tech.*, 64: 295–313 (1989).
18. Wichman, I.S., "Basic Features of Triple Flames in Combustion Theory," to appear *8th ISTP*, July, 1995.
19. Venkatesh, S., Ito, A., and Saito, K., *ME Report*, Dept. of Mechanical Engineering, University of Kentucky, Lexington, KY 40506, 1994.

20. Chung, S.H., and Lee, B.J., **Combust. Flame**, 86: 62–72 (1991).
21. Dold, J.W., **Combust. Flame**, 76: 71–72 (1989).
22. Card, J.M. and Williams, F.A., **Combust. Sci. Tech.**, 84: 91–119 (1992).

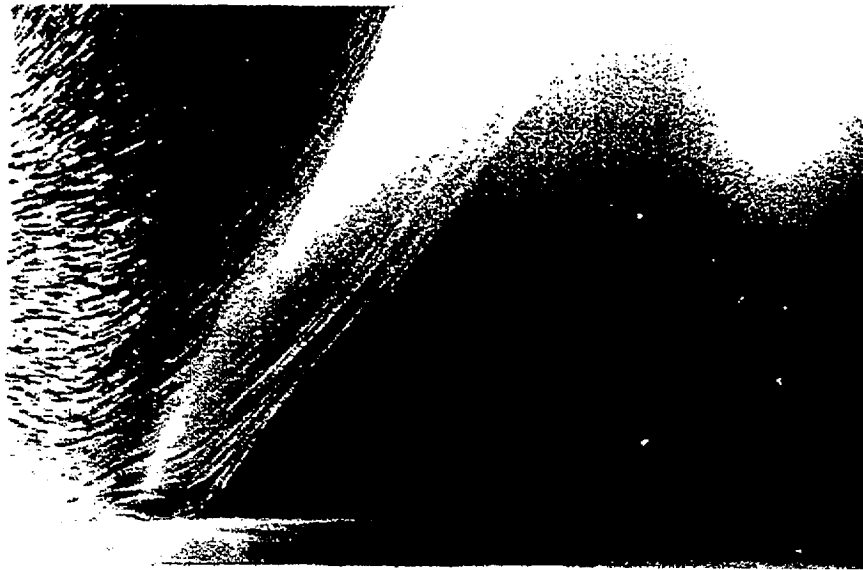
## Figure Captions

- Figure 1** A schematic of the three zone structure for small pool fires and a schematic of particle-track laser-sheet (PTLS) flow visualization apparatus.
- Figure 2** PTLS photographs for the flow fields for a 5.7 cm diameter hexane pool fire: (a) at and around PAZ, and (b) inside the flame sheet and near the fuel surface.
- Figure 3** Profiles of 2D velocity fields for a 5.7 cm diameter hexane pool fire constructed from the figure 2 results.
- Figure 4** Tangential velocity component,  $V_t$  and normal velocity component,  $V_n$  measured by PTLS along the flame sheet and at different vertical height from the burner port,  $Z$ .
- Figure 5** Radial distribution of the temperature near the base for five different heights: (a) hexane, and (b) 1-propanol. (The thermocouple bead was coated with soot only at  $Z = 10$  mm of the hexane flame; all other points for both propanol and hexane flames are free from the soot deposit).

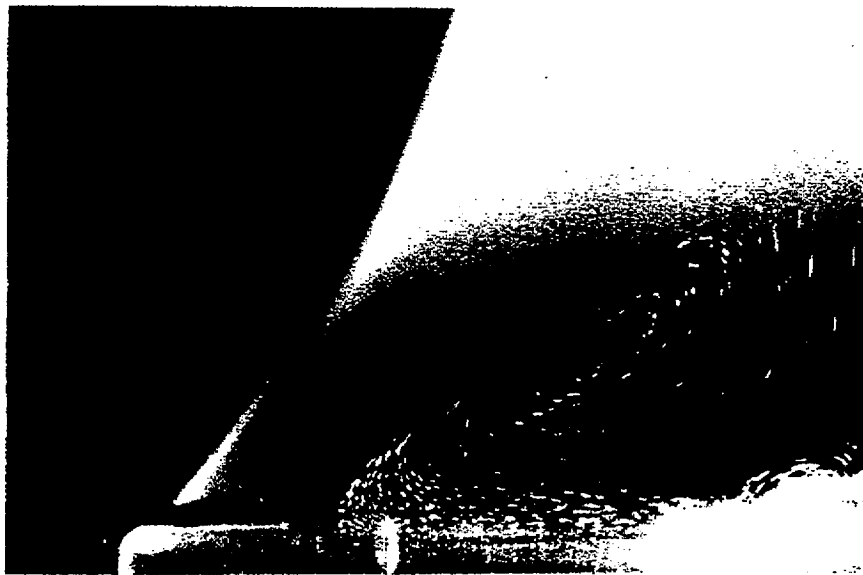


A: Particle feeder  
 B: Control valve

Venkatesh et al Fig. 1

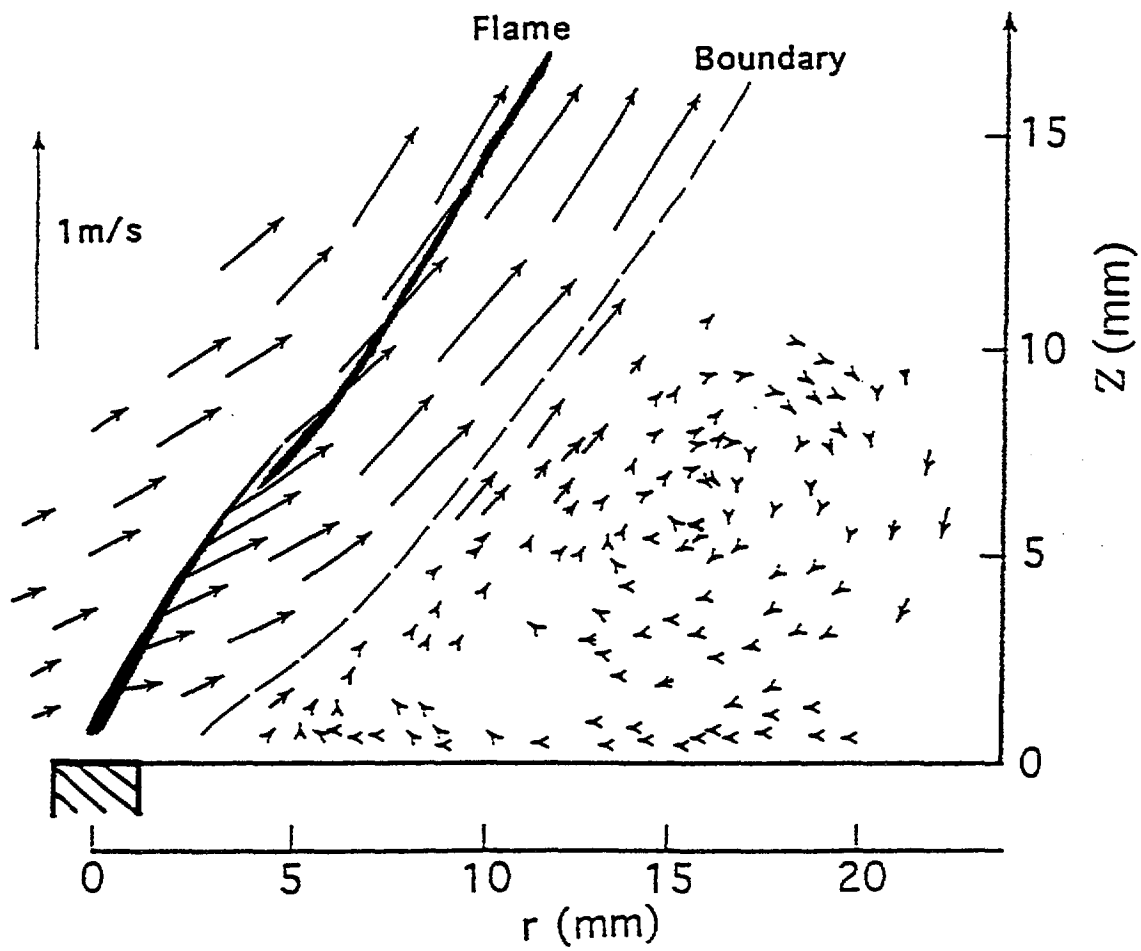


( a )

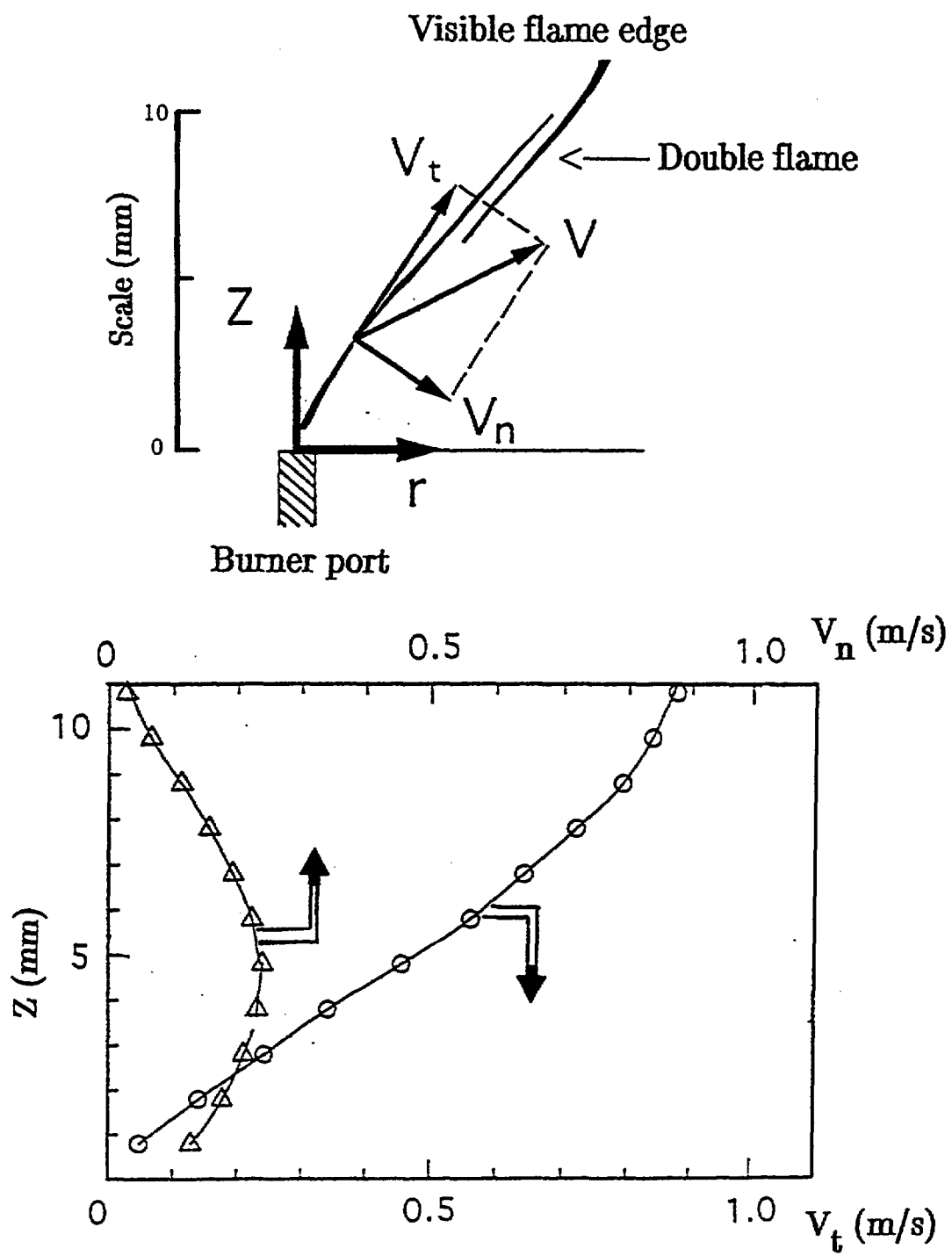


( b )

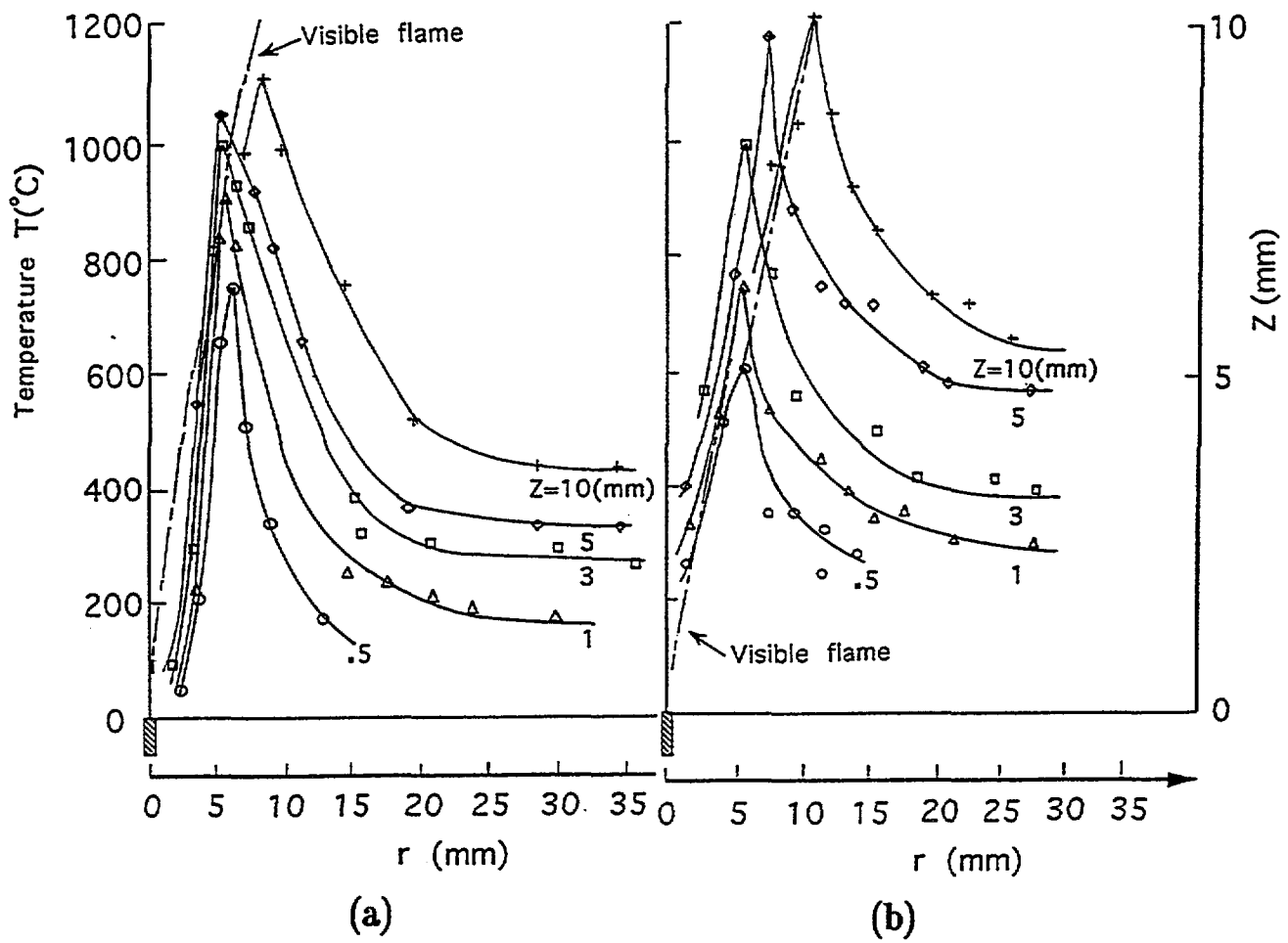
Venkatesh et al Fig. 2



Venkatesh et al Fig. 3



Venkatesh et al Fig. 4



Venkatesh et al Fig. 5.

# The Measurement of Transient 2-D Profiles of Velocity and Fuel-Concentration over Liquids

A. Ito<sup>\*</sup>, A. Narumi<sup>\*\*</sup>, T. Konishi<sup>\*</sup>,  
G. Tashtoush, K. Saito and C.J. Cremers

*Dept. of Mechanical Engineering  
University of Kentucky  
Lexington, KY 40506-0108*

## ABSTRACT

We recently developed two different optical techniques in order to simultaneously measure transient 2-D profiles of velocity, temperature and fuel concentration which were generated by a spreading flame over liquids. The first technique, PTLs, employs a particle-track system combined with a laser-sheet system and a high speed camera, while the second technique employs a dual wavelength holographic interferometer (DWHI). The PTLs system revealed transient 2 D profiles of flame induced flow, while DWHI revealed 2 D profiles of fuel concentration over liquids. In this paper we present a series of velocity profiles for a pulsating flame spread over propanol and concentration profiles for gaseous propanol determined with PTLs and DWHI respectively. Other researchers have predicted the formation of small twin circulations, one a gas-phase circulation just ahead of the flame's leading edge, and the other a small liquid circulation just underneath the gas-phase circulation. Our PTLs results confirmed these predictions, i.e., the formation of a millimeter-diameter circulation in the gas phase and an accompanying liquid flow. Based on these data, we offer a phenomenological explanation of the mechanism of pulsating flame spread. In addition, we show that DWHI is a very promising technique for measuring transient fuel-concentration profiles over liquids.

---

### Present Addresses:

A. Ito and T. Konishi, Dept. of Production Systems Engineering, Oita University, Oita 870-11, Japan, and  
A. Narumi, Dept. of Mechanical Engineering, Kanagawa Inst. of Tech., Atsugi, Japan.

## INTRODUCTION

### Historical Background

The phenomenon of flame spread over liquids is of current interest because of its importance to fire safety. Our objective is different. We wish to learn more about the fundamental mechanism of the flame spread. An excellent review of the literature on this problem was published by Ross [1] and Hirano and Suzuki [2] and the theoretical background of the problem was provided by Williams [3]. They addressed many of the problems that needed to be investigated.

The present paper is a continuation of our previous studies on flame spread over liquids [4-6]. In these studies we applied holographic interferometry (HI) to obtain a detailed and instantaneous temperature distribution in the liquid phase near the fuel surface. In each of methanol, ethanol and propanol we found subsurface-liquid convection in both the uniform spread, and pulsating spread regions. To understand the mechanisms of flame spread in both regions, researchers tried to identify the major heat-transfer process between the flame's leading edge and the liquid, whether it occurs through the gas phase, liquid phase or both. When the liquid convection is produced and it travels ahead of the flame's leading edge, the flame spread is likely to be controlled by it because the convection carries the high temperature liquid ahead of the flame's leading edge. This enhances evaporation of liquid vapor resulting in the formation of a flammable mixture of fuel and air through which the flame can spread. If there is no liquid convection ahead of the flame's leading edge, the major heat transfer can occur between the flame's leading edge and the liquid by conduction and radiation in the gas phase, because conduction through the liquid is negligible [7].

Liquid convection is unique to flame spread over liquids and it complicates the spreading process in comparison to flame spread over solids, which have no condensed phase convection. Thus, it is important to measure temperature and velocity profiles in the liquid phase. Akita [8] was the first researcher to apply a shadowgraph technique to visualize the liquid convection. He reported the formation of liquid convection in the

pulsating region, but no liquid convection in the uniform spread region. Based on Akita's data, Glassman and Dryer [7] proposed that the uniform spread is controlled by heat conduction through the gas phase, while in the pulsating region the liquid convection plays an important role. However, the proposed mechanism for the uniform spread is questionable, because the gas-phase conduction may not transfer sufficient heat for the flame to spread at a rate of nearly 10 cm/s.

To solve this problem, we developed an HI system and performed the transient measurement of liquid temperature [4]. The response time of our HI system is less than 1 microsecond. We estimate the uncertainty of the spatial resolution to be  $\pm 0.1$  mm, and the temperature resolution to be  $\pm 0.1$  °C [4]. Using the HI system, we observed a large liquid convection both in the uniform and pulsating spread regions. The liquid convection in the uniform spread region was a surprise, because the head of the liquid convection preceded the flame's leading edge by approximately 1 cm [4], which is entirely different from Akita's result [8]. To make sure of the accuracy of the data, we repeated the experiments several times and found the reproducibility to be within  $\pm 90$  %. Thus, we proposed a new mechanism: the flame spread in the uniform spread region is governed by the liquid convection [4]. However, at that time we did not really understand why Akita's shadowgraph results were so different from our HI results.

Later, Howard Ross's group at NASA Lewis Research Center applied rainbow schlieren deflectometry (RSD) to measure liquid convection generated by the spreading flame [9]. They found little liquid convection ahead of the flame's leading edge in the uniform spread region. Their RSD data were similar to Akita's shadowgraphs and disagreed with our HI results. Over the past three years, both NASA and our group have tried to understand the reasons for the disagreement, but failed to do so until a series of parametric experiments was completed. In those experiments, the effects of six different parameters were investigated: sensitivity of both RSD and HI systems, impurity of propanol (if any), the relative humidity of the air, the ambient air temperature, several different types of ignition method, and finally different tray widths. We found that the

first five parameters had little influence on the disagreement. However, when we checked the effect of tray width (0.5, 1, and 2 cm) on the liquid convection, the least suspected parameter, a surprising result emerged: the 0.5 cm wide tray had a large liquid convection in the uniform spread region, while the trays that were 1 cm and 2 cm wide had a thin layer of liquid convection. It was so thin and small that only a very sensitive measurement technique could detect it. The result for the 2-cm tray was very similar to the NASA's result for the 2-cm tray. A closer look at their RSD result also revealed a small and thin layer of liquid convection that was always ahead of the flame's leading edge. Comparison of these findings led us to the agreement that in the uniform spread region there is always a small liquid convection indicating that the major heat transfer is by that mode. It also became clear that the shadowgraph [8] did not detect the liquid convection because the size of the liquid convection was too small and beyond the limitation of the spatial resolution of the shadowgraph. Later we applied the shadowgraph technique and proved this explanation.

The validity of this new mechanism has already been proven for the tray that is 0.5 cm wide [4] and extended to one that is 4 cm wide. Beyond that width there are no experimental data, but we speculate that the mechanism will be sustained up to a certain tray width; a hypothesis that will be investigated in the future by both NASA and our group. In the end, both NASA and our group shared Neils Bohr's message "We will never understand anything until we have some contradictions."

Howard Ross's group is now conducting a series of experiments on flame spread using 2 and 4 cm wide trays under the microgravity condition. They have already obtained interesting results which are yet ready to be interpreted [10]. Our group is also conducting a series of flame-spread experiments using 0.5, 1, 2, 4, and 10 cm wide trays under normal gravity.

### **The Current Problem**

NASA's microgravity test results showed that pulsating spread did not occur in

either shallow or deep pool experiments [1]; instead the flame was extinguished, indicating the importance of the buoyancy effect in the gas phase on the mechanism of pulsation. Schiller and Sirignano, using numerical calculations [11], predicted the existence of a very small circulation in the gas phase ahead of the flame's leading edge. They suggested that the gas-phase circulation, which is unique in the pulsating spread and appears with the liquid-phase circulation, may play an important role in flame pulsation [11,12]. There are LDV flow measurement data obtained with Laser-Doppler Velocimetry (LDV) by Santoro et al. [13] showing a gas-phase circulation of approximately 1-cm diameter in the pulsating spread region. However, their LDV result is rather a qualitative indication of the formation of circulation.

To confirm the prediction [11,12] and understand the role of the small gas-phase circulation in the flame pulsation, transient velocity profiles in the gas phase just above the liquid surface and just ahead of the flame's leading edge must be measured. These measurements are not easy, because the rate of flame spread varies from a few centimeters to a few tens of centimeters per second and the target region, where detailed velocity profiles are needed, is at most a few millimeters in diameter.

Previously we learned that LDV was not sufficiently accurate for our measurements [14]. Instead we used PTLs to measure flow profiles in 2D with a spatial resolution on the order of a millimeter in the primary anchoring region of a small pool fire [14]. Based on that experience, we applied the same technique to measure a time series of detailed velocity profiles in the pulsating spread region. As a result, we confirmed the formation of a small circulation approximately in the same location as predicted by the UCI numerical model [11]. We also confirmed, in agreement with the model prediction, that the formation of a small circulation appeared only in the pulsating spread region.

To further advance our understanding of the flame spread over liquids, the direct measurement of propanol concentration over the liquid just ahead of the flame's leading edge was conducted using DWHI. Our DWHI data are accurate when the flow of the gas phase flow has a 2-D profile. When the flow profile shifts from the 2D to 3D, our current

DWHI system will lose its accuracy. To overcome this limitation, we are working on the development of an advanced 3-D-DWHI system.

## **EXPERIMENTAL METHODS**

### **Test Apparatus for Flame Spread**

The flame-spread apparatus (Fig. 1) used for this study is essentially the same as that used in a previous flame-spread study [4-6]. A Pyrex tray with variable width (0.5, 1, 2, and 4 cm) x 2 cm deep x 30 cm long was used. The two long sides of the fuel tray were made of Pyrex of 0.2-cm thickness. The entire liquid tray was enclosed in an open top Pyrex test cell 14 cm high x 15 cm wide x 35 cm long in order to minimize laboratory draft and provide a repeatable flame-spread condition.

Propanol was used as fuel, since it provides a common database for us to use for comparison of our data with NASA's microgravity data [1,9] and our previous experiments [4-6]. The fuel was uniformly ignited at one end by a small pilot flame. To measure the velocity of the liquid convection, we sprinkled aluminum particles of 5- $\mu\text{m}$ -diameter onto the liquid surface. That the aluminum particles float on the liquid surface and follow closely the direction of the liquid-flow convection was confirmed by comparing a time series of simultaneous interferograms for both gas and liquid phases with the video taped behavior of the aluminum particles [5]. A chromel-alumel thermocouple with a 50- $\mu\text{m}$  diameter was used to measure the initial liquid temperature. High pressure nitrogen was supplied from a nitrogen cylinder to extinguish the flame. The talc-particle feeding system is the same as the one used in the previous study [14].

### **Velocity Measurement with a Particle Track and Laser Sheet System (PTLS)**

From our previous studies [14,15], we learned that a PTLS technique with a high speed video camera having a speed of 5,000 frames/s and a view angle of 25 degrees can best serve our measurements. The PTLS can measure profiles of both stream lines and 2-D velocity profiles with significantly fewer particles and nearly instantaneously. Using a

6-W Ar-ion laser-beam and a cylindrical lens, we established a 1 mm thick sheet of laser light with an approximately 35 degree opening angle (Fig. 1). The laser beam was guided by an optical fiber. A beam stabilizer was used to eliminate small fluctuations in the power output of the laser. Prior to ignition, the gas phase above the open top fuel surface was seeded with talc particles with a mean diameter of  $3 \pm 1 \mu\text{m}$  determined by scanning electron microscope.

The trajectories of these particles were recorded by a high speed video camera which was connected to a video system and a TV monitor for the real time observation of both flow field and spreading flame.

### Dual Wavelength Holographic Interferometry (DWHI)

The basic principles behind DWHI are the same as those for the single HI [4-6]. A schematic of DWHI is shown in Fig. 5. DWHI is an indirect measurement technique with a response time of less than a microsecond and a spatial resolution of less than  $\pm 0.1$  mm in identifying concentration difference. The DWHI has significant advantages over the microsampling technique, which has a spatial resolution of several millimeters and a response time that is at best on the order of a second. In addition, the microsampling technique is a direct technique that will cause a large physical disturbance in the flow field [16].

In the present study we use a 2-D model of DWHI and experimentally determine the best possible 2-D condition for the measurement. Details will be given in the following section. Because the basic principles of DWHI are detailed in [17, 18], we will provide only the equations for the temperature and the fuel concentration, respectively.

$$T = \frac{(3P/2R) [N_{A\lambda_1} (N_B - N_A)_{\lambda_2} - N_{A\lambda_2} (N_B - N_A)_{\lambda_1}]}{[(n-1)_{\lambda_1} (N_B - N_A)_{\lambda_2} - (n-1)_{\lambda_2} (N_B - N_A)_{\lambda_1}]}$$

$$C = \frac{[(n-1)_{\lambda_2} N_{A\lambda_1} - (n-1)_{\lambda_1} N_{A\lambda_2}]}{[(n-1)_{\lambda_1} (N_B - N_A)_{\lambda_2} - (n-1)_{\lambda_2} (N_B - N_A)_{\lambda_1}]}$$

The symbols  $N$  and  $n-1$  in these equations are respectively defined as:

$$N = X_{\text{fuel}}N_{\text{fuel}} + (1 - X_{\text{fuel}})N_{\text{air}}$$

and

$$n-1 = 3/2(P/RT)[N_{\text{air}} + X_{\text{fuel}}(N_{\text{fuel}} - N_{\text{air}})].$$

The other symbols are:  $T$  = temperature,  $X_i$  = mole fraction of species  $i$ ,  $P$  = pressure,  $M_i$  = molar refractivity of species  $i$ ,  $R$  = universal gas constant for fuel vapor,  $W_i$  = molecular weight of species  $i$ ,  $\lambda_1$  = wavelength of laser beam 1 (Green Ar-ion laser-beam), and  $\lambda_2$  = wavelength of laser beam 2 (He-Ne laser-beam).

DW holograms contain holograms of two different wavelengths that need to be separated, one corresponding to the temperature difference and the other to the density difference. We first recorded the holograms on a high sensitivity film. Then, during the printing process, two different filters were used to separate the two holograms. These filters have narrow band-pass widths, each passing the wavelength match to that of its respective laser-beam.

## RESULTS AND DISCUSSION

### PTLS Results

A schematic of the pulsating flame spread consisting of six different steps is shown in Fig. 2. Step (a) is the beginning of the cycle of pulsation and the process moves on to steps (b), (c), ( $d_1$ ), ( $d_2$ ), (e), and returns to step (a) to complete the cycle. The schematic of step ( $d_1$ ), not shown in the original diagram published in 1991 [4], was added because it helps us understand the process of flame pulsation better.

At both steps (a) and (b), the flame is at rest and heat is transferred from the flame to the liquid; step (a) is the initial step and (b) represents a further developed state such that the size of the liquid-convection cell at (b) is larger than that at (a). During this preheating process, the temperature difference in the liquid increases as a function of time

setting up step (c). At step (c), the temperature difference in the liquid became large enough to generate a surface tension driven flow, i.e., when the original liquid convection CCZ reached a certain mean diameter, it produced a new liquid convection, STF. The thickness of STF is approximately one third that of CCZ. Just after STF is generated, the flame suddenly moved forward (step  $d_1$ ) indicating that the fuel concentration ahead of the flame's leading edge satisfied the lean flammable limit (the assumption of the formation of the lean flammable mixture is important, thus we measured it by DWHI). When the flame reached the head of CCZ, it stopped (step  $d_2$ ). A few seconds later, the step (e) took place. Then the process returned to the step (a). The holograms corresponding to the steps (a), (b), (c), ( $d_1$ ) and (e) were published in [4]. Five different vector diagrams corresponding to 2-D flow under the conditions of (a, b, c,  $d_1$ , and  $d_2$ ) in Fig. 2 are shown in Figs. 3. The flow diagram for step (e) is not shown, because it is similar to that of step (a). Figure 4 shows a vector diagram for a 2-D flow obtained in the uniform spread region, and the corresponding schematic of the uniform spread. All the flow diagrams mentioned here (Figs. 3 a-d and 4) were obtained from the high speed video films and were averaged over at least several trials (reproducibility was excellent).

Figures 3 (a) and (b) do not show any circulation in the gas phase. When the process progressed to Fig. 3 (c), an interesting result occurred: a millimeter-diameter circulation in the gas phase between the flame's leading edge and the liquid surface appeared. At the same time, the aluminum particles on the liquid also moved forward indicating the initiation of liquid convection (likely a surface tension driven flow). This process is also schematically depicted in Fig. 2. When the flame moved forward again, the processes corresponding to the small gas-phase circulation, Figs. 3 ( $d_1$ ) and ( $d_2$ ), disappeared. Thus, our experimental results agree very well with the theoretical predictions made by Schiller and Sirignano [11,12]. We also conducted the same experiment in the uniform spread region and no clear gas-phase circulation was obtained (Fig. 4). However, a vector diagram of the flow (Fig. 4) shows the existence of a source of expansion, which is located just ahead of the the flame's leading edge. This indicates the

possibility of existence of a small gas-phase circulation. This possibility will be further investigated in the future.

### DWHI Results

High speed video and IR photographs taken from above the tray revealed that for the 0.5 cm wide tray, both the surface-temperature distribution and the shape of the flame front are parabolic in nature, while for the 1, 2 and 4 cm wide trays, small twin circulations were generated on the fuel surface [10] suggesting that the character of the flow profile of the gas phase flow profile is changed from 2D to 3D by increasing the width of the tray. A recent study by Garcia-Ybarra [19] also suggested the 3-D nature of the gas-phase flow induced by a spreading flame over alcohols. To increase the accuracy of the DWHI, the 3-D effect needs to be minimized. We experimentally did this by taking a series of video pictures together with DW holograms and identifying the best 2-D-flame shape from the video film and corresponding DW hologram.

Figure 6 shows a combined DW hologram in the uniform spread region, and Fig. 7 shows two different holograms: (a) an Ar-Ion-laser-beam hologram, and (b) a He-Ne-laser-beam hologram obtained in the pulsating spread region. Figure 8 shows profiles of the temperature and propanol concentration obtained from the holograms of Fig. 7 in the pulsating flame-spread region corresponding to Fig. 3 (c). Figure 8 shows that the propanol concentration in the propanol-air mixture just ahead of the flame's leading edge is within the lean flammability limit. This verifies the assumption made by both Glassman and Dryer [7] that the mechanism of pulsating flame spread is the alternation of two different flame-spread processes: the flame spread in a premixed gas layer and the flame spread driven by a subsurface-liquid convection. We also obtained two DW holograms: one corresponding to the condition of Fig. 2 (a) and the other corresponding to Fig. 2 (b), and applied the same procedure to obtain propanol concentrations in the gas phase just ahead of the flame's leading edge. We found that the mole fraction of propanol in the propanol-air mixture was less than 2.2%, which was below the lean flammability limit.

Again our result confirms the pulsating spread mechanism proposed by Glassman and Dryer [7].

It should be noted that our DWHI assumes a 2-D model and the pulsating flame spread consists of spreads by a blue finger (or clawing) flame and a main luminous flame, in which the finger-flame spread is rather unstable. The applicability of the 2-D-model assumption to this flame needs to be further investigated.

## SUMMARY AND CONCLUSIONS

(1) Previously, we developed a unique PTLs system for measuring velocity profiles for transient flow in a very limited space. We applied this PTLs system to study the mechanism of the pulsating flame spread over propanol and successfully obtained a series of PTLs flow diagrams. These PTLs flow diagrams revealed a gas-phase circulation on the order of 1-mm diameter in the pulsating spread region together with a liquid-phase convection, both of which were predicted by other researchers.

(2) Gas-flow profiles induced by a spreading flame over the liquid change from 2D to 3D with increasing tray width. Accordingly, the structure of the liquid convection may change by increasing the tray width. Thus the effect of the tray width on the spread mechanism needs to be investigated in the future.

(3) We applied the DWHI system to measure transient profiles of the gas-phase-propanol concentration over the liquid-propanol surface. We obtained a series of DW holograms and confirmed that the flame spread occurred only when the propanol concentration is within the lean flammability limit. Our current DWHI assumes a 2-D model, thus the accuracy of the DWHI needs to be improved when it is applied to 3-D problems.

(4) Our DWHI results also show that the mechanism of pulsating flame spread over propanol consists of two different processes: a flame spread through a lean flammable propanol-air mixture and a flame spread driven by a subsurface-liquid convection. Our DWHI also show that the propanol concentration just ahead of the flame's leading edge is within the lean flammability limit. This is further evidence that in the uniform spread

region the subsurface-liquid convection exists and generates a flammable propanol-air mixture above the fuel surface.

## ACKNOWLEDGEMENTS

This study was supported in part by the National Institute of Standards and Technology under Grant #60NANB4D1674, in part by the NASA-Kentucky EPSCoR Program, in part by the Japanese Ministry of Education under US-Japan Collaborative Agreement Travel Grant, and in part by the Center for Manufacturing Systems at the University of Kentucky under a matching grant. We would like to thank H. Ross and F. Miller of NASA Lewis Research Center for providing us with their experimental data and many stimulating discussions.

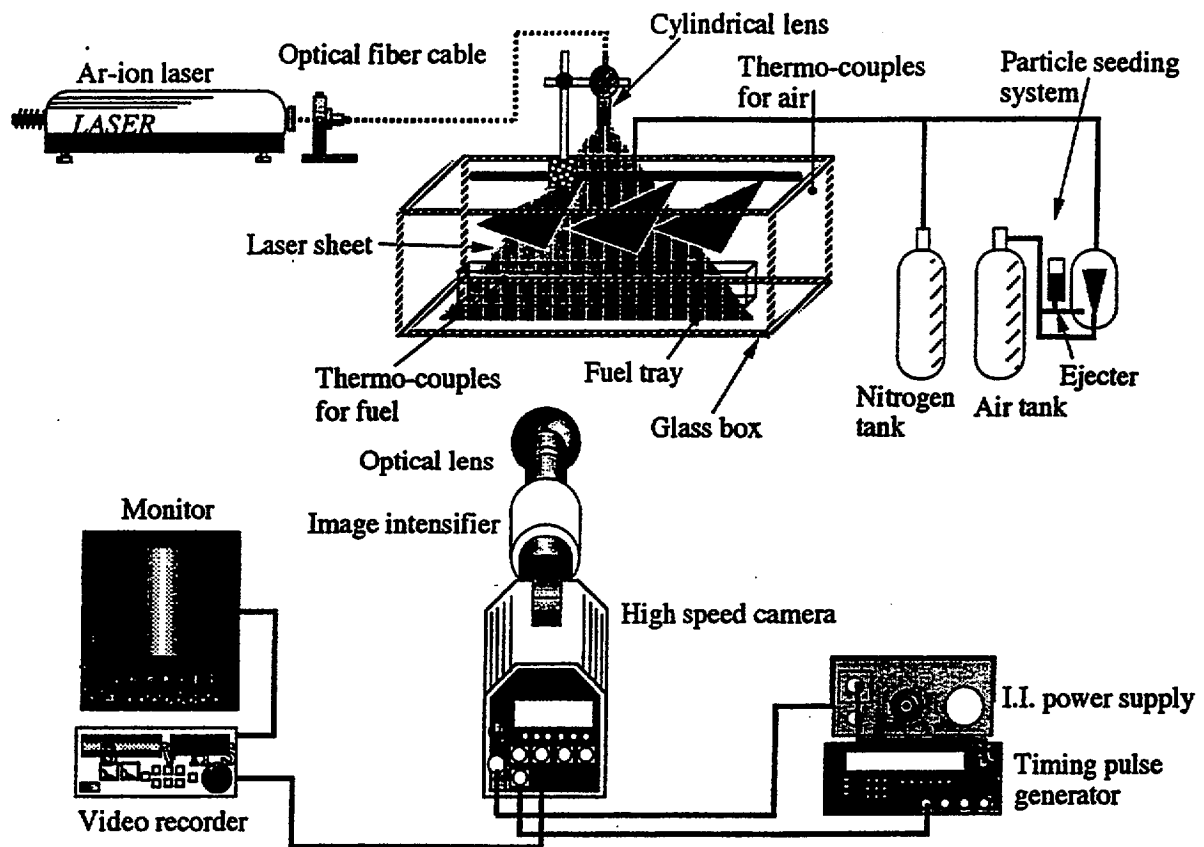
## REFERENCES

1. Ross, H.D., *Prog. Energ. Combust. Sci.*, 20: 17-63 (1994).
2. Hirano, T., and Suzuki, T., *Fire Safety J.*, 21: 207-229 (1993).
3. Williams, F.A., *Combustion Theory, Second Edition*, Benjamin/Cumming, Menlo Park, CA, (1985), Chap. 12.
4. Ito, A, Masuda, D, and Saito, K., *Combust Flame*, 83: 375-389 (1991).
5. Ito, A., Saito, K., and Cremers, C.J., "Pulsating Flame Spread over Liquids," *Fire Safety Science - Proc. Fourth International Symposium*, Edited by T. Kashiwagi, International Association for Fire Safety Science, (1995), pp. 445-456.
6. Tashtoush, G., Narumi, A., Ito, A., Saito, K., and Cremers, C.J., Combined Techniques of Holographic Interferometry and Particle Track Laser Sheet to Study Flame Spread over Liquids," *Eighth International Symposium of Application of Fluid Mechanics*, Lisbon, Portugal, (1996).
7. Glassman, I. and Dryer, F.L., *Fire Safety Journal*, 3: 123-138 (1981).
8. Akita, K., "Some Problems of Flame Spreading along a Liquid Surface," *Fourteenth Symposium (International) on Combustion*, The Combustion Institute, (1972), pp. 1075-1083.
9. Miller, F.J. and Ross, H.D., "Further Observation of Flame Spread over Laboratory-Scale Alcohol Pools," *Twenty-Fourth Symposium (International) on Combustion*, The Combustion Institute, (1992), pp. 1703-1711.

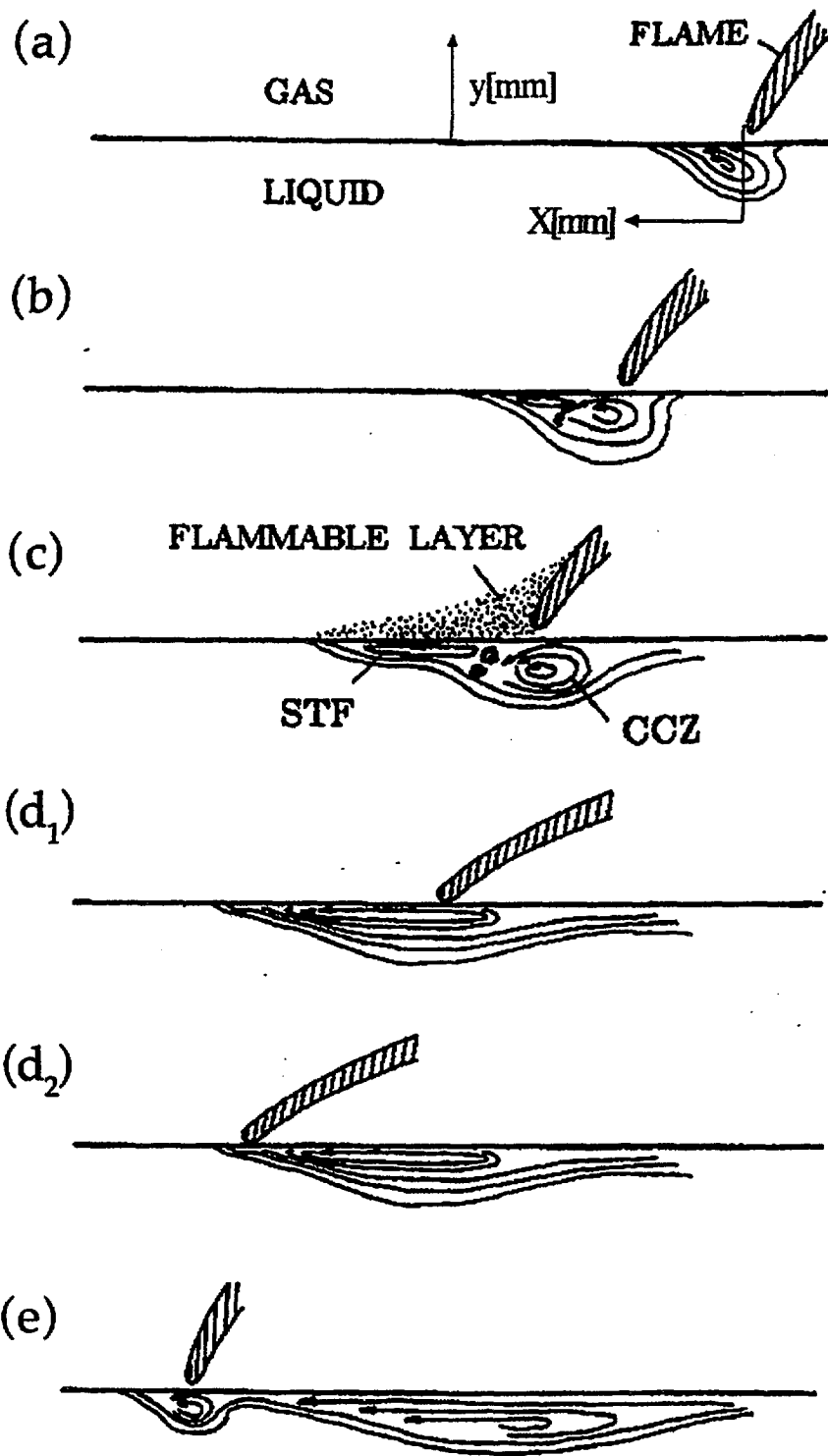
10. Ross, H., and Miller, F.J., "Detailed Experiments of Flame Spread Across Deep Butanol Pools," **Twenty-Sixth Symposium (International) on Combustion**, The Combustion Institute, (1996), to appear.
11. Schiller, D.N. and Sirignano, W.A., *J. Thermophys. Heat Transfer.*, 6: 105-130 (1992).
12. Sirignano, W.A. and Schiller, D.N., *Combust. Sci. Tech.*, (1996), to appear.
13. Santoro, R.J., Fernandez-Pello, A.C., Dryer, F.L., and Glassman, I., *Appl. Optics*, 17: 3843 (1978).
14. Venkatesh, S, Ito, A, Saito, K., and Wichman, I.S., "Anchoring Mechanism of Liquid Pool Fires," **Twenty-Sixth Symposium (International) on Combustion**, The Combustion Institute, (1996), to appear.
15. Hirano, T., and Saito, K., *Prog. Energ. Combust. Sci.*, 20: 461-485 (1995).
16. Saito, K., Williams, F.A., and Gordon, A.S., *J. Heat Transfer*, 108: 640-648 (1986).
17. Spatz, T.L, and Poulikakos, D., *J. Heat Transfer*, 114: 998 (1992)
18. Ito, A., Narumi, A., Saito, K. and Cremers, C.J., "Temperature Measurement in Liquids by Holographic Interferometry," *Proc. Eighth International Symposium on Transport Phenomena on Combustion*, S.H. Chan Edit., (1995), to appear.
19. Garcia-Ybarra, P.L., et al., "Study of the Thermocapillary Layer Preceding Slow Steadily-Spreading Flames over Liquid Fuels," **Twenty-Sixth Symposium (International) on Combustion**, The Combustion Institute, (1996), to appear.

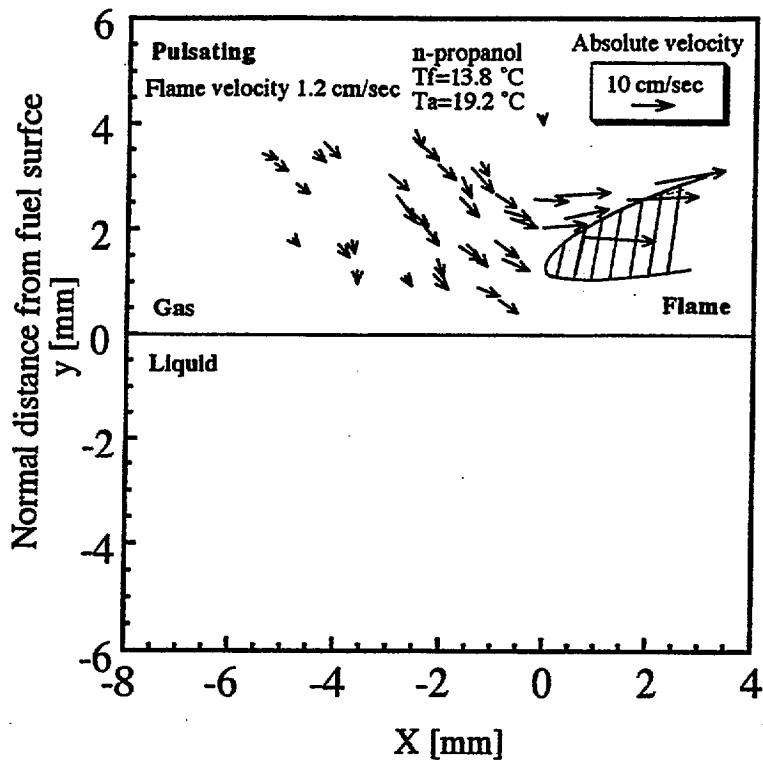
## Figure Captions

- Figure 1** Experimental apparatus of Particle-Track Laser-Sheet (PTLS) system connected to a high speed camera, VCR and TV monitor. Nitrogen was used for flame extinguishment and the particle seeding system is the same as the one used previously (see [14]). The thermocouple was used to measure the initial liquid temperature.
- Figure 2** Schematics of the pulsating flame spread. The original schematics were published in 1991 [4]. STF stands for a surface tension flow, and CCZ for the cold convective zone. This time, an additional step ( $d_2$ ) was added to the original five step (a through e) process.
- Figure 3** Five different PTLS flow diagrams obtained in the pulsating flame spread region over propanol. The initial liquid temperature:  $13.8^{\circ}\text{C}$  and the ambient air temperature:  $19.2^{\circ}\text{C}$ . The captions: (a) through ( $d_2$ ) correspond to the conditions described in Fig. 2.
- Figure 4** A PTLS flow diagram obtained in the uniform spread region over propanol and a schematic of the uniform flame spread process. The initial liquid temperature was:  $18.4^{\circ}\text{C}$  and the ambient air temperature was:  $22.4^{\circ}\text{C}$ .
- Figure 5** A schematic of DWHI system.
- Figure 6** A DW hologram obtained in the uniform spread region (the experimental condition is the same as Fig. 4).
- Figure 7** Two holograms: (a) an Ar-ion laser beam hologram and (b) a He-Ne laser beam hologram, separated from a DW hologram obtained in the pulsating spread region (the experimental).
- Figure 8** Vertical profiles of (a) gas-phase temperature and of (b) mole fraction of propanol, both constructed from the Figs 5 and 6 holograms at two different locations specified in Fig. 6.

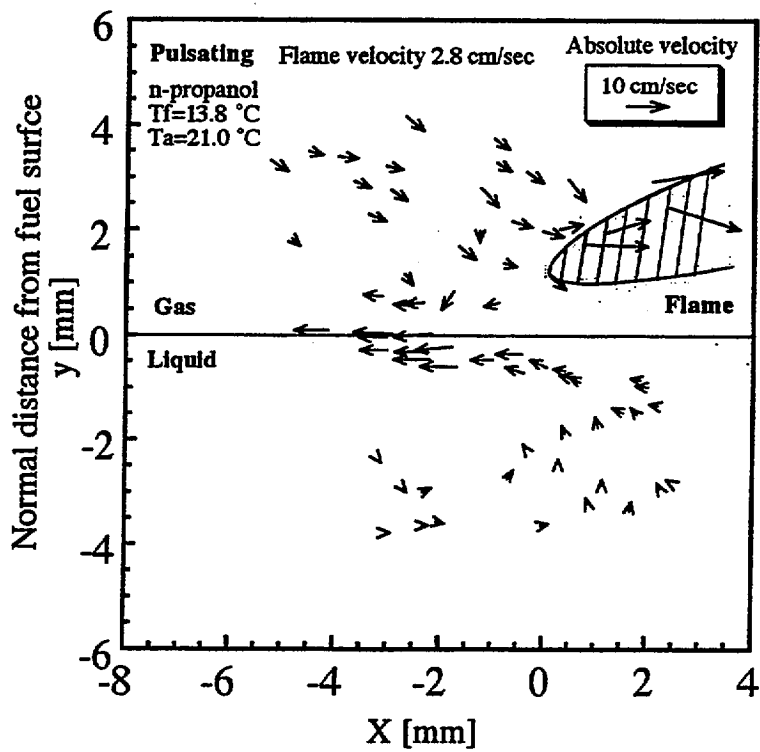


Ito et al - Fig1

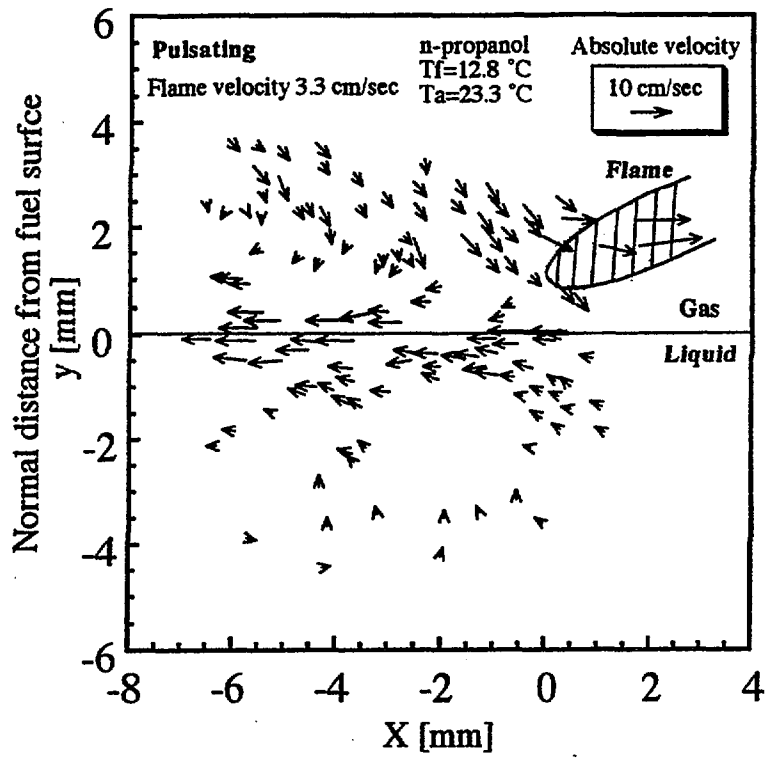




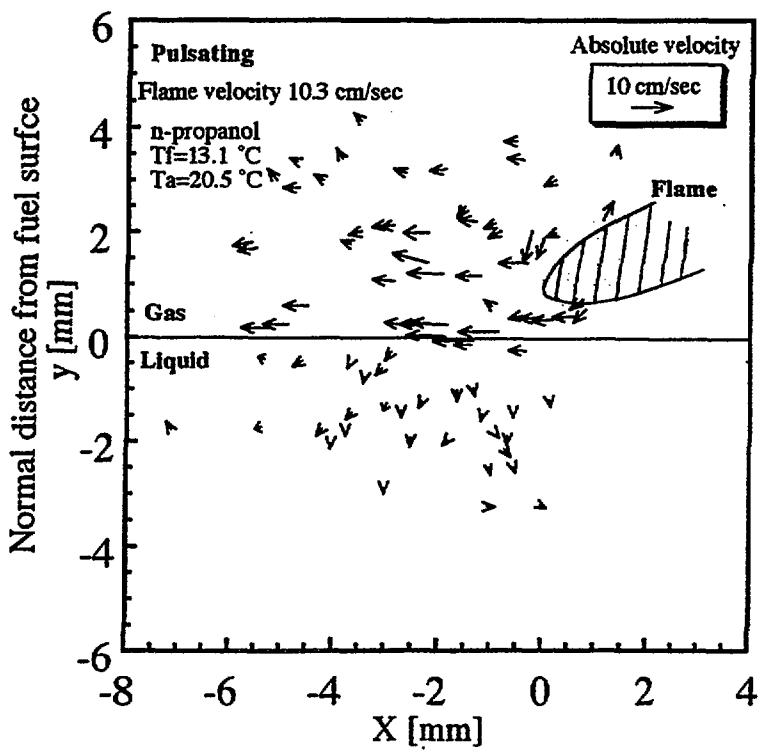
Ito et al - Fig3(a)



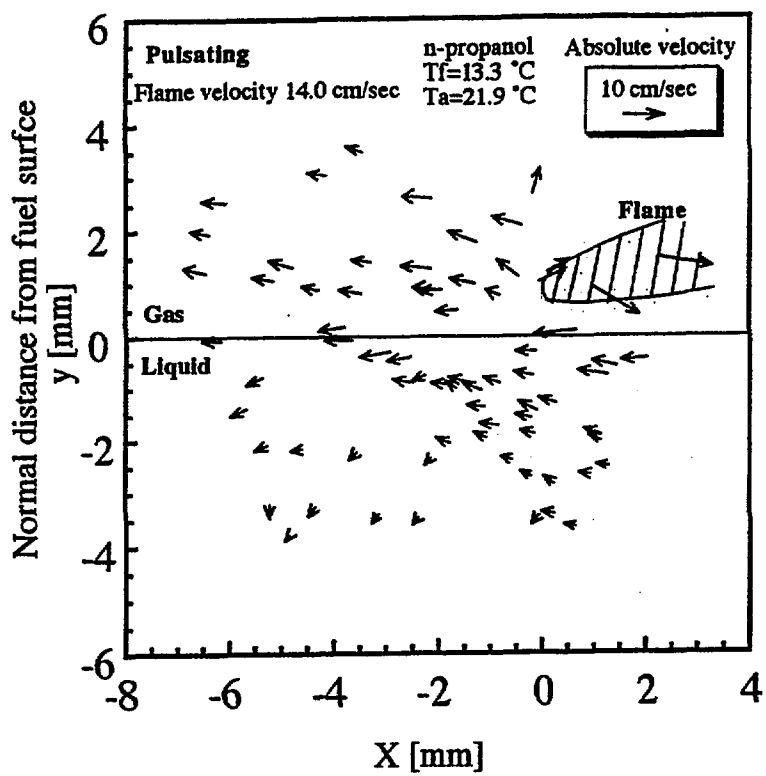
Ito et al - Fig3(b)



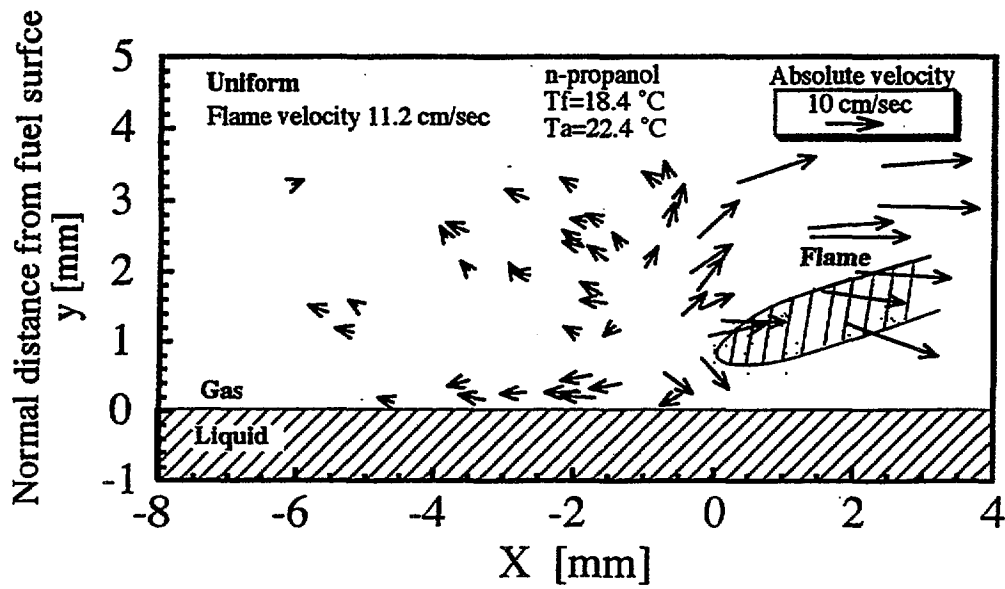
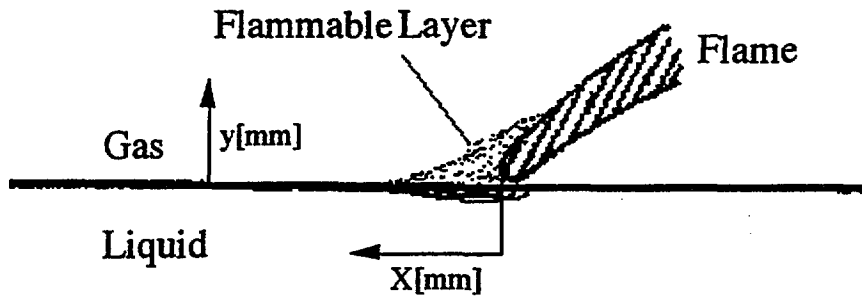
Ito et al - Fig3(c)



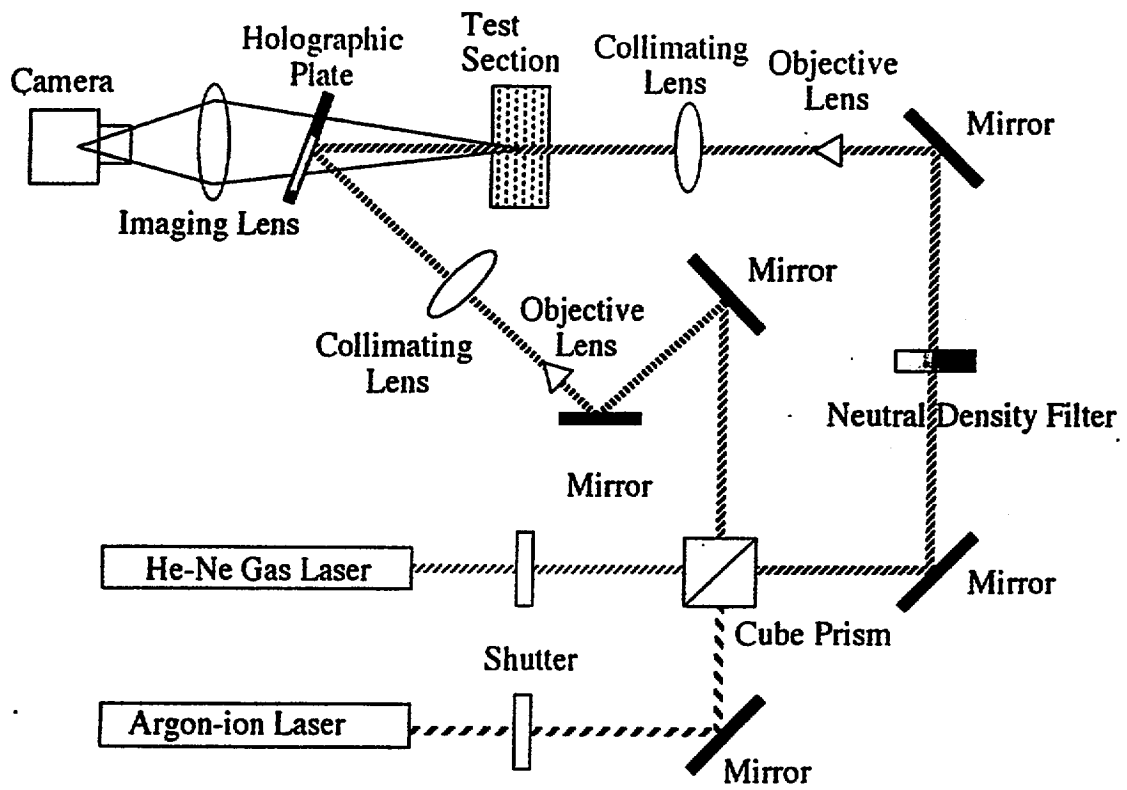
Ito et al - Fig3(d<sub>1</sub>)



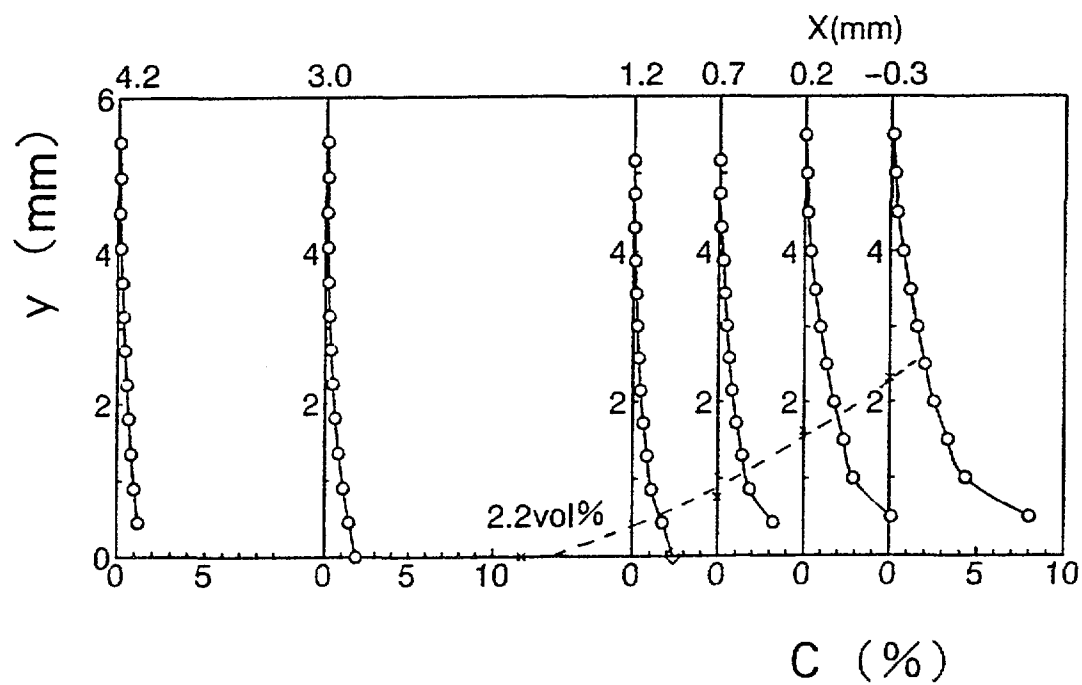
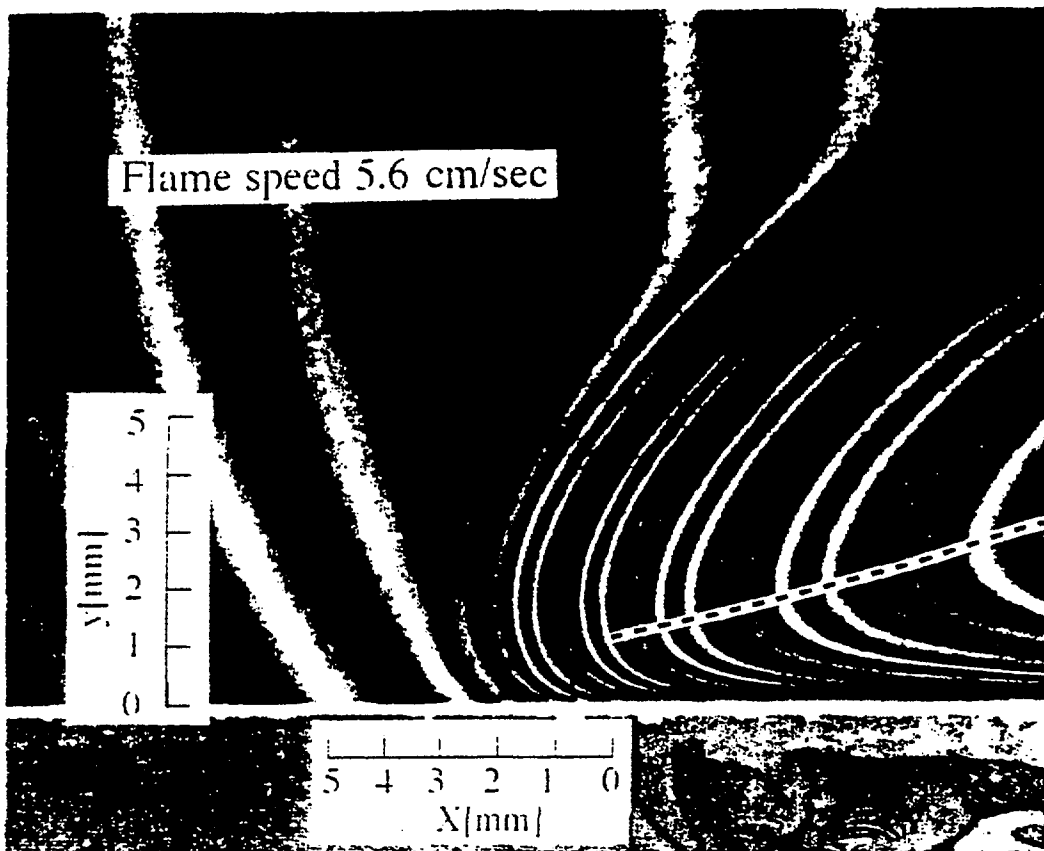
Ito et al - Fig3(d<sub>2</sub>)



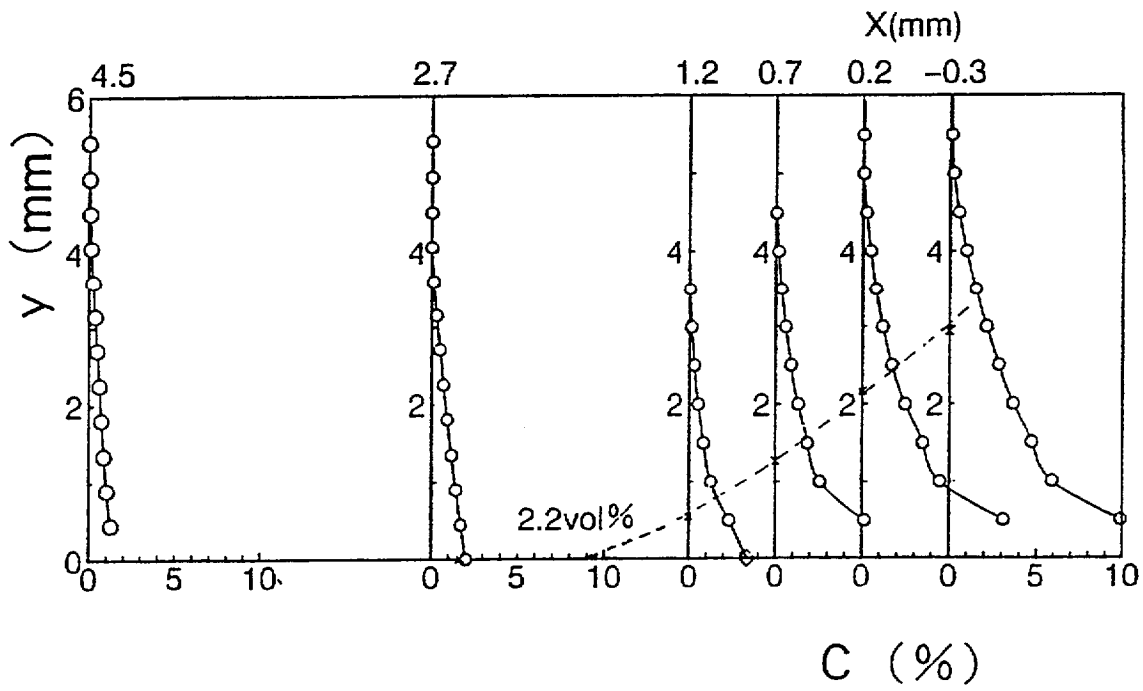
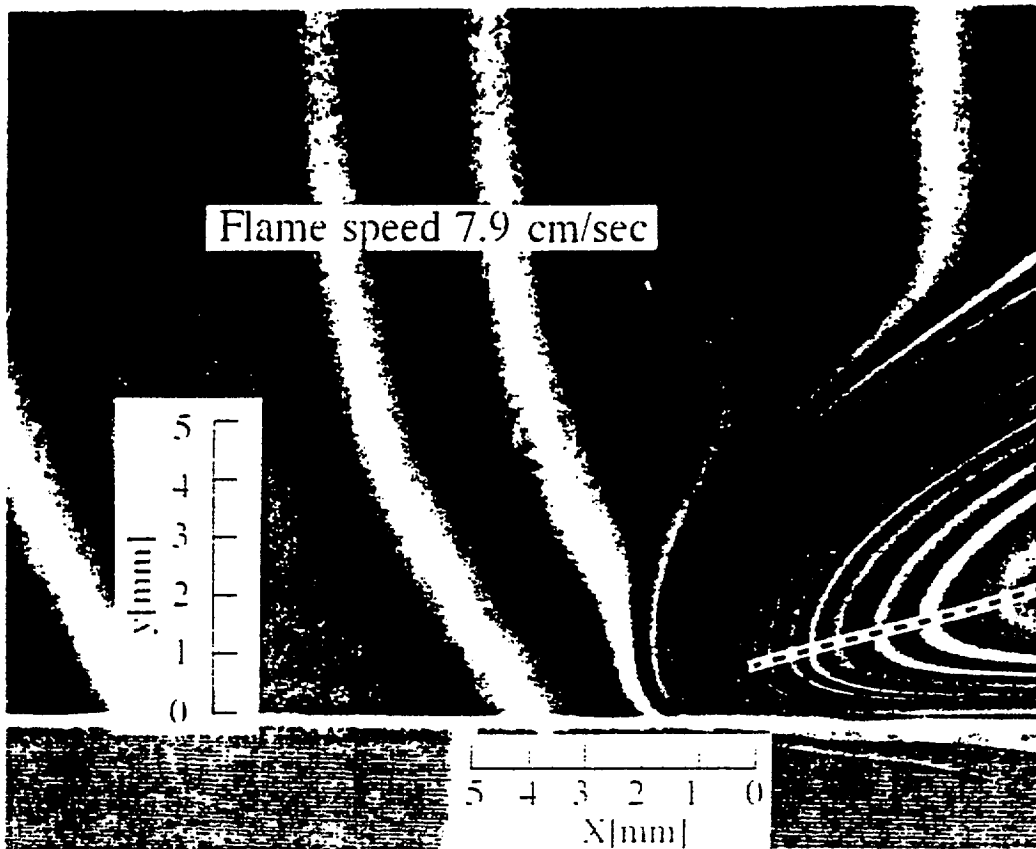
Ito et al - Fig4



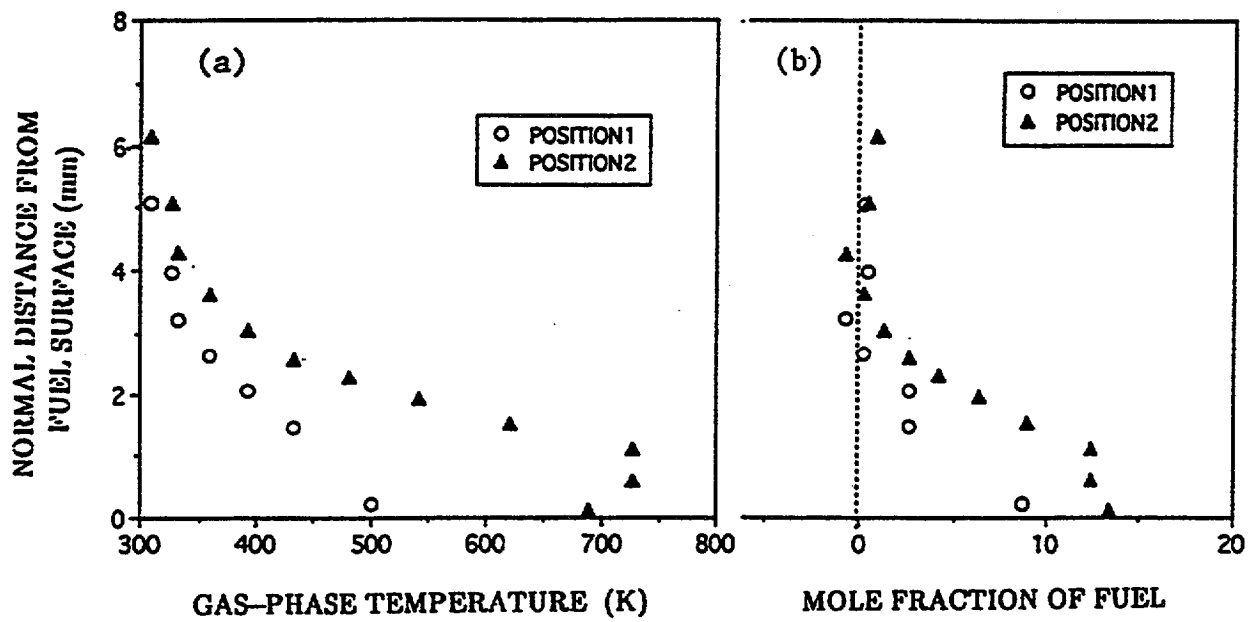
Ito et al - Fig5



Ito et al - Fig6



Ito et al - Fig7



Ito et al – Fig. 8

*This paper was presented at the 8th International Symposium on Transport Phenomena in Combustion, 1995 and will appear in Proceedings edited by S.H. Chan, 1997.*

## **TEMPERATURE MEASUREMENT BY HOLOGRAPHIC INTERFEROMETRY IN LIQUIDS**

Akihiko Ito, Akira Narumi, Kozo Saito and Clifford Cremers  
Department of Mechanical Engineering  
University of Kentucky  
Lexington, KY 40506

### **ABSTRACT**

Detailed temperature measurements of the condensed phase are important for the study of flame spread over liquids and liquid-pool fires leading to boilover. The measurement requires high spatial resolution near the interface between liquid and gas, where a steep temperature gradient is formed and that controls heat-transfer process between the two phases. Conventional thermocouple techniques have limitations on accurate measurements in this type of sensitive location because the thermocapillary effect of the thermocouple bead significantly distorts the original temperature structure near the interface. To avoid such interference, we developed a holographic interferometry (HI) technique that is non-intrusive and is capable of detecting nearly simultaneously a sudden and minute temperature change occurring in a distributed area. The thermo-optical coefficients of liquids are two orders of magnitude higher than that of gases. Therefore, if an interferogram was obtained simultaneously for the interface region between a gas and a liquid, the gas phase hologram is two orders of magnitude less sensitive than the liquid phase hologram. To enhance the sensitivity in the gas phase, a dual wave-length holography was applied. In this study, we show that HI is a very useful temperature measurement technique, and the estimated errors are so small that they cause no significant errors when the HI data are used for quantitative analysis. This paper summarizes recent progress made on the application of HI to highly transient phenomena, such as the studies of flame spread and liquid-pool fires.

### **INTRODUCTION**

As demonstrated in our previous studies on flame spread over liquids [1] and pool fires on liquids [2], an accurate knowledge of the transient temperature profiles in the condensed phase is necessary for the understanding of the control mechanisms of such transient phenomena. This paper summarizes recent results of applying the HI technique to flame spread over liquids and pool fires leading

to boilover [3,4]. An accurate measurement of temperature profiles in the condensed phase requires an instantaneous temperature mapping capability that includes high resolution in space and time and simultaneous collection of spatially distributed signals. A conventional point-by-point measurement technique using a thermocouple, however, is incapable of satisfying these requirements because of the disturbing effects of the wire on the condensed phase, the limited spatial resolution of the thermocouple bead, and the limited response time of the thermocouple [3,4].

A holographic interferometer connected to a photographic recording system can instantaneously detect a sudden and small temperature change occurring over a distributed area. Previously [1] detailed temperature profiles in the subsurface-liquid-convection current were investigated using this technique. Basic principles of this method were given by Ito and Kashiwagi [5], and their applicability was successfully demonstrated for 1-decene by Kashiwagi and Kashiwagi [6] and for polymethylmethacrylate by Ito and Kashiwagi [4]. Previously, detailed temperature profiles in three different alcohols (methanol, ethanol and n-propanol) were measured under a spreading flame condition. The HI study revealed a detailed temperature structure consisting of two counter-rotating circulation zones in the liquid phase under the flame front.

Pool fires leading to boilover were also studied using the HI technique. Boilover, the phenomenon where the water sublayer begins to boil, penetrates the fuel layer, and ejects fuel and water drops into the surroundings, is a complex phenomenon and its mechanism has not yet been fully understood [7,8]. Using the HI technique, we studied the effect of the boiling water sublayer that always occurred prior to the boilover. This study provided detailed temperature distributions in the fuel that overlaid the water and of the fuel-water interface [9], detailed and instantaneous temperature mapping not possible with conventional thermocouple measurement. Based on the HI data, we developed a model to predict the onset time of boilover, which is characterized by the onset of an intense spattering of water and fuel droplets [9].

## **SINGLE WAVE-LENGTH HI**

### **Flame Spread Experiment**

A schematic of the experimental apparatus including fuel trays of 40 cm length, 1 cm height and five different widths (0.5, 1.0, 2.0, 4.0 and 5.0 cm) with a temperature controlled rectangular cooling unit, and a video camera is shown in [1]. The x-coordinate is fixed along the fuel surface (+ downstream of flame front and - upstream of flame front). The y-coordinate is along the vertical direction (+ to air; - to fuel). The z-coordinate is normal to the x-y plane and the origin is fixed to the leading-edge of the moving flame on the fuel surface along the center line of tray. A schematic diagram of the optical system used for holographic interferometry is shown in Fig. 1. Lenses and mirrors are arranged on an optical bench and a 5-mW He-Ne laser was used as the light source. A

refractive index of Pyrex).  $L_s$  is the thickness of Pyrex wall,  $\lambda$  is the wavelength of the laser beam, and  $T_\infty$  is the initial liquid temperature. The thermo-optic coefficient of Pyrex is one order of magnitude smaller than that of the liquid. The thickness of the Pyrex wall is 0.1 cm, which is small compared to the width of the tray. An error estimate was made for the case of Pyrex with 0.1-cm-wall thickness and 0.5 cm width; it was found that the error is not more than 1% of the temperature of the liquid. Therefore, the second term on the left-hand side in Eq. (1) can be neglected.

The reference temperature for the interferogram was obtained with a copper-constantan thermocouple made from 50  $\mu\text{m}$  wire. The spatial resolution for the fringes in interferograms is 30  $\mu\text{m}$ . The accuracy of controlling the liquid temperature is  $\pm 0.5$   $^\circ\text{C}$ . It should be noted that along with the accuracy of our interferogram, the following three effects are important and should be estimated accurately.

(1) The accuracy of the temperature dependence of the estimated thermo-optic coefficient must be obtained. Thermo-optic coefficients for alcohols and hydrocarbon liquids below 25  $^\circ\text{C}$  were investigated experimentally by Hauf and Grigull [10] and theoretically by Murphy and Alpert [11]. However, their temperature dependencies are unknown. Therefore, we measured the thermo-optic coefficients of four different alcohols (methanol, ethanol, n-propanol and n-butanol) as functions of temperature between 2  $^\circ\text{C}$  and 80  $^\circ\text{C}$  using an Abbe refractometer. The measured values were correlated by a quadratic equation. The thermo-optical coefficients were then obtained by taking derivatives and they compared favorably with those at 25  $^\circ\text{C}$  by Hauf and Grigull [10]. The observed difference is less than 1%.

(2) The error due to refraction of light was estimated from the equation described by Ito et al. [12]. The maximum error is estimated to be 0.8  $^\circ\text{C}$  (0.64%) assuming  $(dT/dy) = 250$   $^\circ\text{C}/\text{cm}$  and tray width is 0.5 cm.

(3) The error due to temperature variation in the liquid along the light beam, which is caused by heat loss to the wall, must be measured. The fringe number is determined by integrating the temperature distribution along the path length and dividing it by the path length. The difference between the temperature at the center of the liquid along the path length and the average temperature is less than 1% of the temperature at the center of liquid.

As a result, the estimated total maximum error from steps (1)-(3) above does not exceed 3% of the temperature at the center of liquid; thus, holographic interferometry is accurate enough for us to pursue our objective.

A series of six interferograms for propanol (flash point = 25  $^\circ\text{C}$ ) can be seen in [13]. These interferograms can be used to qualitatively study the flow structure in the liquid phase and temperature structure in the gas phase. However, quantitative information may not be easily deduced from these interferograms due to the three dimensional structure of the subsurface-liquid flow. To demonstrate the HI technique for the use of quantitative analysis, a representative interferogram and an illustration of the corresponding isothermal lines are shown in Fig. 2. The interferogram was taken for flame spread over propanol whose initial temperature was 21  $^\circ\text{C}$  and the flame spreads with a

constant velocity without pulsation. The HI technique revealed a detailed temperature structure in the liquid phase. It is also sensitive enough to detect the subsurface-liquid convection-current. Therefore, quantitative information is available from the interferogram. Based on the interferogram results in Fig. 2 and gas-phase velocity-measurement results by Hirano et al. [14], it was found that gas-phase and liquid-phase-convection currents are important for preheating the liquid ahead of the flame [1]. Our HI found a double circulation structure, a thin layer of subsurface flow and a cold circular convective flow. Both are located underneath the flame leading edge (Fig. 2).

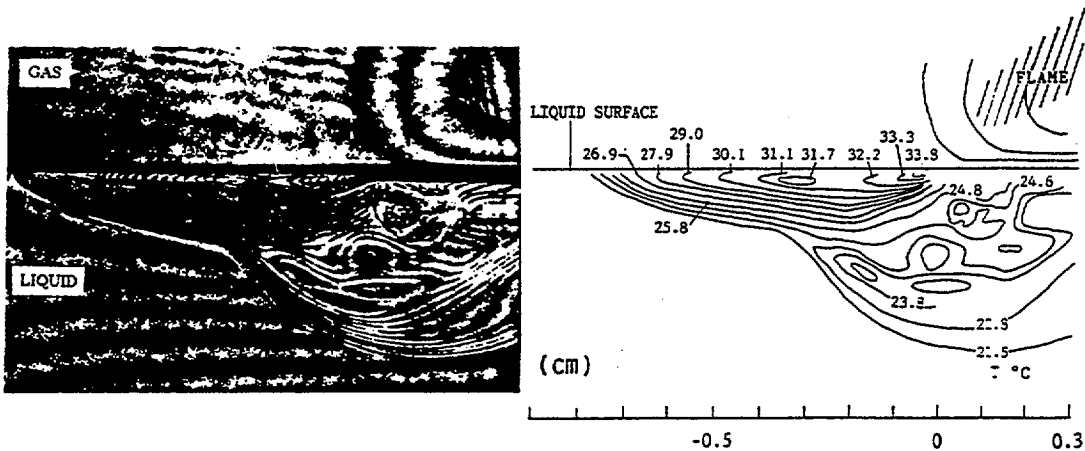


**Figure 2** Liquid temperature-structure obtained by HI and its isothermal lines (1-propanol with initial liquid temperature, 21°C).

### Boilover Experiment

Rectangular Pyrex containers were used [2] and a 35 mm motor driven camera with a telephoto lens was used to record the hologram with a shutter speed of 1/500, which was fast enough to "freeze" the diffraction image. Interferograms were taken at 1 to 0.1-s intervals depending on the phenomenon of interest. The optical system is the same as the one used for the flame-spread experiment (Fig. 1). The diffraction image was enhanced by increasing the intensity of the light so that a real time method could apply as demonstrated previously in the flame-spread experiments.

At the early stages of combustion, the liquid loses heat to the Pyrex free board. With continued combustion, the increased free board area is heated by the flame, and hence the heat is transferred back to the liquid. These effects can create a temperature gradient along the laser beam, causing errors when temperatures are determined from the interferograms. To estimate this effect, copper-constantan thermocouples made of 50- $\mu\text{m}$ -diameter wire were placed in the liquid and the Pyrex wall. The thermocouple wires were horizontal to the

fuel surface to minimize conduction loss. It was found that the temperature distribution in the Pyrex walls does not affect the results. The other errors involved in our HI system are estimated to be at most 3% as shown in the section on the flame-spread experiment.

An interferogram is shown in Fig. 3. which is related to the onset of boilover, at 197 s after the ignition. Two dark lines can be identified; one is between the fuel and the water, and the other is between the gas phase and fuel surface. These dark lines are the result of steep temperature gradients which are beyond the capability of our HI temperature resolution. For  $t < 40$  s, the interferograms revealed that a very steep temperature gradient existed only in the vicinity of the fuel surface, which was approximately 2 mm thick, and that a very gradual temperature change occurred in the water layer. At  $t = 136$  s, the fuel layer shows dynamic motion consisting of small and large eddies. At the onset of boilover,  $t = 197$  s, the entire fuel surface and the fuel-water interface are physically distorted. The distortion may be attributed to a dynamic effect of the superheated water sublayer due to sudden vapor expansion. The temperature at the fuel-water interface was determined from the interferogram to be 376 K. The actual temperature may be slightly higher than this because of the effect of deflection of light along the y-direction and the edge effect. The interferograms at  $t = 197$  s and 202 s show that the strong convective motion generated in the water layer causes uniform temperature profiles in the fuel and water layers near the fuel-water interface.

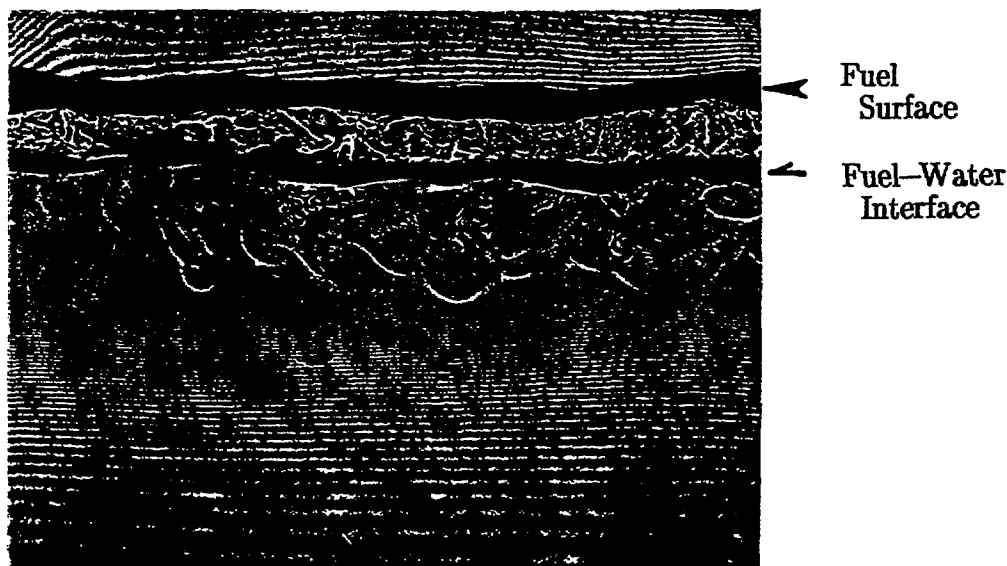


**Figure 3** An interferogram obtained at time,  $t = 197$  sec. after ignition (n-decane with liquid temperature,  $21^{\circ}\text{C}$ ).

## Dual Wave-Length HI

In the past, flame spread over liquids was studied as a function of initial liquid temperature [15-17]. When it is below the flash point, three different spread regimes are observed: those are in the order of decreasing the liquid temperature: (1) uniform spread regime, (2) pulsating spread regime, and (3) quasi-uniform spread regime. According to the definition of flash point, when the liquid temperature is below the flash point, flame spread is not possible; but it can be achieved by preheating the liquid by an ignition source. Once a flame is initiated on the liquid surface, heat will be transferred from the flame to the liquid, raising the local liquid temperature above the flash point. There are two different types of flash point that can be experimentally determined: open-cup flash-point and closed-cup flash-point. If the flame spread is tested under open-cup conditions, the liquid temperature should be below the open-cup flash-point. However, a problem arises when the open-cup flash-point is experimentally determined, because it easily fluctuates several degrees around the average value; likely due to the fluctuation of gas-phase fuel-concentration.

This may cause confusion when experimental results are interpreted by blindly accepting the ill defined open-cup flash-point. One believed to be a below flash-point result may well be one above the flash-point. This problem can be solved, however, if gas-phase fuel-concentration is monitored during the experiment. A micro-sampling technique is well established for species concentration measurement for stationary flames, but it may not be feasible for spreading flame, because it requires sampling time of at least several seconds.

What we propose here is a dual wavelength holographic interferometry (DWHI), an indirect technique whose response-time is less than a microsecond with spatial resolution less than 0.1 mm in identifying concentration difference (the corresponding spatial resolution for the micro-sampling is at best on the order of several millimeters). It also can be applied to three dimensional problems.

In this study we use a two dimensional model because our experimental condition approximates that state. The index of refraction,  $n(x,y,\tau)$  can be written as:

$$[n - n_{\infty}] L = m\lambda . \quad (2)$$

Here  $L (= L_1 + L_2)$  is tray width, and the rest of symbols are explained earlier. Using the Lorentz-Lorenz equation, Eq. (2) can be rewritten as:

$$(1/\rho) [(n^2-1)/(n^2+2)] = N/M. \quad (3)$$

Here  $N$  = molar refractivity, and  $M$  = molecular weight. Using the equation of state for an ideal gas and  $n \approx 1$ ,

Flame spread experiments were conducted using a 4 cm wide tray filled with 1-propanol, the same apparatus used previously. A representative DW hologram is shown in Fig. 5, which is much more detailed and clearer than that for the single wavelength HI in Fig. 2. A few interesting aspects from this interferogram can be discussed.

(1) The interferogram in Fig. 5 shows an integrated temperature distribution along the laser beam. Previously, a high speed-video picture and IR photograph were taken for the flame spreading over the liquid [20,21]; they confirmed that the flame shape was approximately two dimensional (no significant difference along the beam) and liquid-surface temperature along the beam was also sustained nearly uniform (the largest temperature variation near the edge was

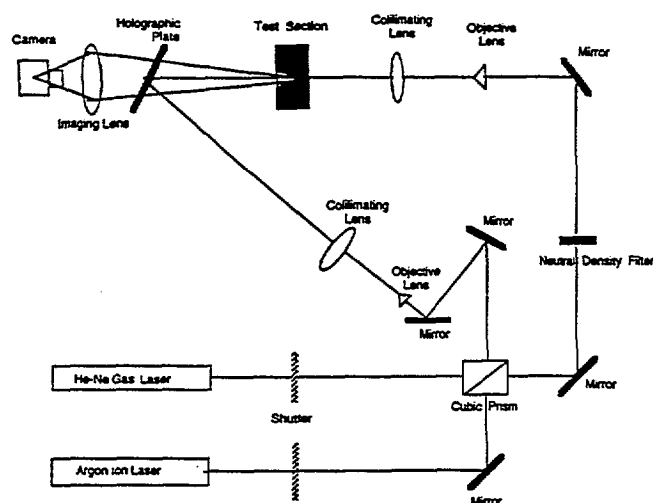


Figure 4 A schematic of DWHI.

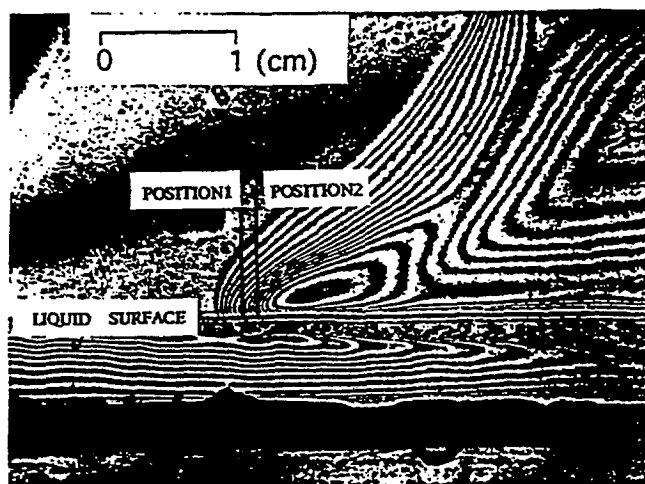
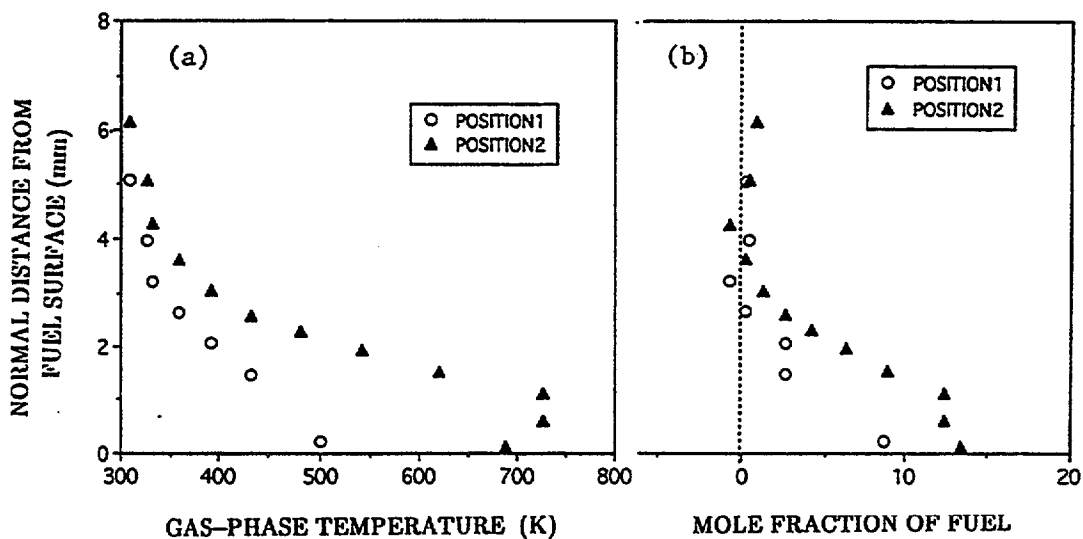


Figure 5 A DW interferogram taken for spreading flame over 1-propanol at initial liquid temperature, 21°C.

20% different from the center line value). Therefore, along the beam we expect approximately the same percentage variation in gas-phase temperature, which is not significant.

(2) There are two different fringe groups which are separated by a circular fringe zone. The one front of the circular shape is the main spreading flame, while the one behind the circular zone is part of a pulsating flame (precursor flame or finger flame [16]) which can be separated from our discussion here. The maximum temperature gradient location is located just in front of the circular fringe zone. The maximum temperature gradient is likely to occur on the fuel-lean side adjacent to the maximum flame-temperature location. Therefore, the flame-front location may be found somewhere between the maximum temperature-gradient location and the circular fringe zone. Formation of the circular fringe zone was also found in stationary pool fires [22,23], and so it is not unique to the spreading flame. It can be interpreted as a buoyancy-driven convection which is caused by a sudden expansion of the fuel vapor near a high temperature flame-zone.



**Figure 6** Vertical profiles of (a) gas-phase temperature and of (b) mole fraction of fuel, both constructed from the figure 5 HI at two different locations specified in the figure 5.

Figure 6 shows gas-phase temperatures and fuel-vapor concentrations, both measured at positions 1 and 2 as shown in Fig. 5, as a function of height from the fuel surface,  $y$ . The result in figure 6 is straightforward, since a narrow band-pass filter can eliminate fringes due to the change of fuel-vapor concentrations. The same procedure that was employed for the liquid temperature measurement was applied to obtain the result in Fig. 6. The result in Fig. 7 was obtained by assuming the gas-phase composition is only air and fuel vapor; however, this assumption may not be accurate because combustion by-products and fuel-pyrolysis products (generated in a high temperature region) can diffuse or convect

to the measurement location. Fortunately, because the measurement location is upstream from the flame front location and their temperatures are relatively low, the above assumption may not cause a substantial error. When the above assumption is not valid, a further complicated process is required to reduce the concentration data from DWHI, which is beyond the scope of this paper and will be discussed in Ref. [24].

## CONCLUSIONS

(1) The HI technique was proven to be a very effective tool in nearly simultaneously obtaining a detailed and temporal temperature map over a region about the fuel-gas interface for studying both flame-spread and pool-fire phenomena.

(2) The single wavelength HI can accurately detect transient liquid-temperature profiles; while DWHI can detect transient profiles of both temperature and fuel concentrations in the gas phase. The thermocouple point-by-point temperature-measurement technique has limitations due to its spatial resolution; and species concentration measurement by micro-sampling has limitations due to both its spatial resolution and time response.

(3) Dual wave-length HI has proven to be a very useful technique for simultaneously measuring transient profiles of both temperature and fuel concentrations in the gas phase. When both combustion by-products and fuel-pyrolysis products affect the fuel concentrations, the accuracy of this technique for measuring the fuel concentrations decreases. Therefore, further work is needed to solve this problem.

## ACKNOWLEDGEMENTS

We wish to acknowledge H. Ross and F. Miller of NASA Lewis Research Center for valuable technical discussions on flame spread over liquids, and M. Majidi and G. Tashtoush for their technical assistance during HI measurements. This study was in part supported by the National Institute of Standards and Technology under Grant #60NANB4D1674, in part by Kentucky NASA EPSCoR Program (NCCW-60), and in part by the Center for Robotics and Manufacturing Systems of the University of Kentucky.

## REFERENCES

- [1] A. Ito, D. Masuda and K. Saito, *Cumbustion and Flame*, 83: 375 (1991).
- [2] A. Ito, K. Saito and T. Inamura, *J. Heat Transfer*, 114: 944 (1992).
- [3] J.S. Newman, Laser Doppler Velocimeter Measurements of the Gas and Liquid Flow Fields Induced by Flame Propagation over a Liquid Fuel Surface, *MSE Thesis, Mech. and Aerospace Engineering Dept., Princeton*

- University, Princeton, NJ (1979).
- [4] A. Ito and T. Kashiwagi, *Combustion and Flame*, 71: 189 (1988).
  - [5] A. Ito and T. Kashiwagi, *Applied Optics*, 26: 954 (1988).
  - [6] T. Kashiwagi and T. Kashiwagi, *Nineteenth International Symposium on Combustion*, The Combustion Institute, p. 1511 (1984).
  - [7] D. Evans, G. Mulholland, D. Gross, H. Baum and K. Saito, Environmental Effects of Oil Spill Combustion, *Report NISTIR 88-3822*, National Institute of Standards and Technology, Gaithersburg, MD 20899, (1988).
  - [8] D. Evans, G. Mulholland, D. Gross, H. Baum and K. Saito, Burning, Smoke Production, and Smoke Dispersion from Oil Spill Combustion, *Report NISTIR 89-4091*, National Institute of Standards and Technology, Gaithersburg, MD 20899, (1989).
  - [9] T. Inamura, K. Saito and K.A. Tagavi, *Combustion Science and Technology*, 86: 105 (1992).
  - [10] W. Hauf and U. Grigull, *Advances in Heat Transfer*, Series 6, Academic Press, p. 268 (1970).
  - [11] C.G. Murphy and S.S. Alpert, *Journal of Physics*, 39: 834 (1974).
  - [12] A. Ito, S.K. Choudhury and T. Fukano, *Transaction of JSME*, Series B, 56: 194 (1990).
  - [13] A. Ito, K. Saito and C.J. Cremers, *Fire Safety Science - Proc. Fourth International Symposium*, The International Association for Fire Safety Sciences, pp. 455-456 (1994).
  - [14] T. Hirano, T. Suzuki, I. Mashiko and N. Tanabe, *Combustion Science and Technology*, 22: 83 (1980).
  - [15] K. Akita, *Fourteenth International Symposium on Combustion*, The Combustion Institute, p. 1075 (1972).
  - [16] H. Ross, *Progress in Energy and Combustion Science*, 20: 17 (1992).
  - [17] I. Glassman and F.L. Dryer, *Fire Safety Journal*, 3: 123 (1980).
  - [18] W.C. Gradiner, Jr., Y. Hidaka and T. Tanazawa, *Combustion and Flame*, 40: 213 (1981).
  - [19] T.L. Spatz and D. Poulidakos, *J. Heat Transfer*, 114: 998 (1992).
  - [20] F. Miller and H. Ross, Temperature Field During Flame Spread over Alcohol Pools: Measurements and Modeling, *Presented at the Eastern States Section, The Combustion Institute Meeting*, Florida, November (1994).
  - [21] A. Bouhafid, J.P. Vantelon, P. Joulain and A.C. Fernandez-Pello, *Twenty-second International Symposium on Combustion*, The Combustion Institute, pp. 1291-1298 (1988).
  - [22] S. Venkatesh, A. Ito and K. Saito, Why are Pool Fires Anchored?, submitted to *Combustion and Flame*, (1994).
  - [23] A. Narumi, G. Tashtoush, K. Saito and C.J. Cremers, Dual Wave-Length HI, to be published.

NIST-114 (REV. 11-94) ADMAN 4.09	U.S. DEPARTMENT OF COMMERCE NATIONAL INSTITUTE OF STANDARDS AND TECHNOLOGY	(ERB USE ONLY)	
<b>MANUSCRIPT REVIEW AND APPROVAL</b>		ERB CONTROL NUMBER	DIVISION
		PUBLICATION REPORT NUMBER	CATEGORY CODE
INSTRUCTIONS: ATTACH ORIGINAL OF THIS FORM TO ONE (1) COPY OF MANUSCRIPT AND SEND TO THE SECRETARY, APPROPRIATE EDITORIAL REVIEW BOARD.		PUBLICATION DATE	NUMBER PRINTED PAGES
TITLE AND SUBTITLE (CITE IN FULL) Flame Base Structure of Small-Scale Pool Fires			
CONTRACT OR GRANT NUMBER Grant #60NANB4D1674	TYPE OF REPORT AND/OR PERIOD COVERED Final Report		
AUTHOR(S) (LAST NAME, FIRST INITIAL, SECOND INITIAL) Venkatesh, S., Ito, A., Saito, K.	PERFORMING ORGANIZATION (CHECK (X) ONE BLOCK) <input checked="" type="checkbox"/> NIST/GAITHERSBURG <input type="checkbox"/> NIST/BOULDER <input type="checkbox"/> JILA/BOULDER		
LABORATORY AND DIVISION NAMES (FIRST NIST AUTHOR ONLY)			
SPONSORING ORGANIZATION NAME AND COMPLETE ADDRESS (STREET, CITY, STATE, ZIP) U.S. Dept. of Commerce National Institute of Standards and Technology Gaithersburg, MD 20899			
PROPOSED FOR NIST PUBLICATION <input type="checkbox"/> JOURNAL OF RESEARCH (NIST JRES) <input type="checkbox"/> MONOGRAPH (NIST MN) <input type="checkbox"/> LETTER CIRCULAR <input type="checkbox"/> J. PHYS. & CHEM. REF. DATA (JPCRD) <input type="checkbox"/> NATL. STD. REF. DATA SERIES (NIST NSRDS) <input type="checkbox"/> BUILDING SCIENCE SERIES <input type="checkbox"/> HANDBOOK (NIST HB) <input type="checkbox"/> FEDERAL INF. PROCESS. STDS. (NIST FIPS) <input type="checkbox"/> PRODUCT STANDARDS <input type="checkbox"/> SPECIAL PUBLICATION (NIST SP) <input type="checkbox"/> LIST OF PUBLICATIONS (NIST LP) <input checked="" type="checkbox"/> OTHER GCR <input type="checkbox"/> TECHNICAL NOTE (NIST TN) <input type="checkbox"/> NIST INTERAGENCY/INTERNAL REPORT (NISTIR)			
PROPOSED FOR NON-NIST PUBLICATION (CITE FULLY) <input checked="" type="checkbox"/> U.S. <input type="checkbox"/> FOREIGN	PUBLISHING MEDIUM <input type="checkbox"/> PAPER <input type="checkbox"/> CD-ROM <input type="checkbox"/> DISKETTE (SPECIFY) _____ <input type="checkbox"/> OTHER (SPECIFY) _____		
SUPPLEMENTARY NOTES			
ABSTRACT (A 2000-CHARACTER OR LESS FACTUAL SUMMARY OF MOST SIGNIFICANT INFORMATION. IF DOCUMENT INCLUDES A SIGNIFICANT BIBLIOGRAPHY OR LITERATURE SURVEY, CITE IT HERE. SPELL OUT ACRONYMS ON FIRST REFERENCE.) (CONTINUE ON SEPARATE PAGE, IF NECESSARY.) This paper attempts to answer the question, "Why are small scale pool fires anchored?" by providing and interpreting a new set of experimental data. For momentum-controlled, high Reynolds (Re) number turbulent-jet diffusion flames, the formation of a premixing zone is suggested as the primary reason for the flame anchoring. For buoyancy-controlled pool fires, however, the existence of the premixing zone at the flame base is not clear because both Re and Fr (Froude number) are low. To improve our understanding of the flame anchoring mechanism and structure of buoyancy-controlled liquid pool fires, we employed small scale pool fires whose diameters range between 1.5-20 cm. Our measurements include flow visualization by a particle-track laser-sheet technique (PTLS) combined with a high speed video camera and temperature profiles by a fine thermocouple.			
KEY WORDS (MAXIMUM OF 9; 28 CHARACTERS AND SPACES EACH; SEPARATE WITH SEMICOLONS; ALPHABETIC ORDER; CAPITALIZE ONLY PROPER NAMES) air entrainment; diffusion flames; flame spread; flow visualization; pool fires; small scale fire tests; temperature profiles			
AVAILABILITY <input checked="" type="checkbox"/> UNLIMITED <input type="checkbox"/> FOR OFFICIAL DISTRIBUTION - DO NOT RELEASE TO NTIS <input type="checkbox"/> ORDER FROM SUPERINTENDENT OF DOCUMENTS, U.S. GPO, WASHINGTON, DC 20402 <input checked="" type="checkbox"/> ORDER FROM NTIS, SPRINGFIELD, VA 22161		NOTE TO AUTHOR(S): IF YOU DO NOT WISH THIS MANUSCRIPT ANNOUNCED BEFORE PUBLICATION, PLEASE CHECK HERE. <input type="checkbox"/>	

